A C-terminal HaloTag Impairs AGO2 Function

Kunal M. Shah*[1], Alex F. F. Crozier*[1], Anika Assaraf[1], Muzjda Arya[1], Paulo S. Ribeiro[2], Michael J.Plevin[#3] and Tyson V. Sharp[#1]

1. Centre for Cell and Molecular Biology, Barts Cancer Institute, Queen Mary University of London, John Vane Science Centre, Charterhouse Square, London EC1M 6BQ.

2. Centre for Tumour Biology, Barts Cancer Institute, Queen Mary University of London, John Vane Science Centre, Charterhouse Square, London EC1M 6BQ.

3. York Structural Biology Laboratory, York Biomedical Research Institute, Department of Biology, University of York, York YO10 5DD, UK.

* These authors contributed equally
# Corresponding Authors: t.sharp@qmul.ac.uk
michael.plevin@york.ac.uk

Abstract

A full understanding of RNA silencing requires appropriate molecular biology tools to explore the roles of Argonaute 2 (AGO2) and the RNA-induced silencing complex (RISC). Commonly used approaches to study RNA silencing and RISC, such as those relying on affinity tagging and antibodies, have important limitations that can lead to artificial results. Both the N- and C-terminal domains of AGO2 have been shown to be important for correct activity and yet the consequences of appending tags to either terminus have not been fully investigated. N-terminal tags are frequently used to study AGO(2) biology. Recently, an N-terminal *HaloTag-Ago2* fusion was reported and examined in mice. While the versatile HaloTag provided new opportunities to study RISC biology, the tagged construct showed certain activity changes compared to unmodified Ago2. CRISPaint, a new CRISPR-Cas9 technique, offers a route to the accurate and efficient generation of endogenous C-terminal tag fusions. Here, we used CRISPaint to generate the first reported recombinant AGO2 construct with a C-terminal tag: an endogenous C-terminal HaloTag fusion to AGO2 (*AGO2*^{HALO}) in human (A549) cells. We found that the AGO2^{HALO} fusion protein retains the capacity to interact with the key protein binding partner TNRC6A and that the C-terminal HaloTag does not affect cell viability. However, the *AGO2*^{HALO} fusion significantly impairs RNA cleavage and RNA silencing activity compared to control cells, and reduces nuclear localisation of the fusion protein. We conclude that the fusion of a C-terminal HaloTag to AGO2 is not appropriate for studying AGO2 and RISC. Our results stress the importance of fully validating recombinant tagging strategies to ensure that any results generated do not obscure critical functional defects.

Introduction

The four human Argonaute proteins (AGO1-4) are key components of the miRNA-induced silencing complex (RISC), which is critical for the correct regulation of gene expression through microRNA-mediated silencing.[1,2,3,4,5,6,7] Due to the considerable scientific and clinical interest in RNA silencing, a significant body of work has been performed to develop experimental tools for the study of AGO protein function. However, assay design has been limited by methods that rely on antibodies and affinity/autofluorescent tags, which can be technically challenging to use and often lack the sensitivity or specificity required to generate appropriately robust results.

Recombinantly tagging a protein of interest is a widely used strategy in molecular biology and biotechnology for the purification, visualisation, and manipulation of target proteins. To overcome challenges related to antibody specificity and pull-down efficiency attempts to study RISC have often used overexpressed, recombinantly-tagged AGOs. Such approaches, however, carry the risk of generating artefacts. For example, a Flag-tagged AGO2 construct resulted in five-fold over-expression compared to endogenous AGO2 levels, altered AGO2 sub-cellular localisation and resulted in the identification of potentially false binding partners.[8] Such artefacts might arise from either over-expression of the transgene or the presence of the Flag tag itself.[9] Moreover, it has been shown that recombinantly-tagged, over-expressed proteins can non-specifically localise to processing (P) bodies.[10] Caution should therefore be applied to any study that uses recombinantly-tagged proteins, particularly when at greater than physiological levels, to show that both AGO and TNRC6 proteins are strongly localised to P bodies.[10] Consequently, approaches that tag endogenous proteins are often deemed more desirable, although this too can disrupt normal protein function.[11,12] In rapidly proliferating cell lines, endogenously tagged AGOs have been shown to elute as complexes of more variable size than native AGOs, which primarily elute as components of high molecular weight complexes.[13,14] An endogenous N-terminal EGFP-AGO2 fusion protein was not recognised by a pS387-AGO2-specific antibody in immunofluorescence assays, conceivably due to the tag altering AGO2 conformation and therefore reducing pS387 antibody binding.[15] Even in cases where endogenous tags have been shown to retain core RISC activity, these tagged proteins should only be used to study known RISC functions under specific experimental conditions and periods of expression. The use of novel tags and tagging strategies in different cell models may affect the target protein to different, unknown and unpredictable extents. Nevertheless, protein tagging has the capacity to greatly expand our ability to study RNA silencing and RISC proteins, and (manageable) technical biases are inevitable when probing complex biological systems. To confidently exploit the potential benefits that recombinant tagging of endogenous proteins offers, it is important to ensure that the core functionalities of the proteins of interest are sufficiently retained, primarily through considered design and stringent validation, and that technical biases should be considered and minimised when designing experiments and interpreting results.

The HaloTag protein fusion platform is a modular protein tagging system that can be programmed for different functions, proving a versatile technology.[16,17,18] The modified 33-kDa haloalkane dehalogenase HaloTag protein can covalently bind to synthetic chloroalkane ligands (collectively known as HaloTag ligands) which comprise a chloroalkane linker attached to a variety of useful molecules, such as fluorescent dyes, affinity handles, or solid surfaces. Covalent bond formation between the protein tag and the chloroalkane linker is high affinity, rapid, specific and essentially irreversible. This enables efficient purification of HaloTag fusion proteins and means this single genetic construct can have multiple capabilities to comprehensively analyse protein function and interaction. Importantly, an endogenous fusion of HaloTag to the N-terminus of *Ago2* (HaloTag-Ago2) has enabled the high-resolution identification of miRNA targets in mice.[14]

Applying UV crosslinking to cells expressing HaloTag fusion proteins enables efficient identification of RNA targets of RNA-binding proteins.[19] Of note, HaloTag-Ago2 fusions have been used to investigate the association of Ago proteins with RNA in a process termed Halo-Enhanced Ago2 Pulldown sequencing (HEAP-seq).[14] The HaloTag ligand conjugated to a resin can be used to pull down the fused complex in cells or tissues expressing HaloTag-fused AGO. High-throughput sequencing of RNA extracted from purified AGO-miRNA-mRNA

complexes then enables the identification of miRNA-mRNA networks under physiological (and/or pathological) conditions. In addition to bypassing the need for radiolabelling, immunoprecipitation, and gel purification, the covalent nature of the interaction between the HaloTag and its ligand simplifies the isolation of AGO-miRNA-mRNA complexes, removing the intrinsic variability of antibody-based approaches and, as the strong covalent bond permits more stringent washing, there is less potential for non-specific pulldown (while maintaining high sensitivity). Accordingly, HEAP-seq was demonstrated to enable both more sensitive and specific identification of AGO protein-RNA interactions than conventional methods which rely on the use of antibodies to precipitate AGO-containing complexes (i.e. CLIP-seq[20]). Moreover, the HaloTag labelling capacity can also be used to perform live-cell single-molecule imaging to observe dynamic activity and high-resolution investigation of protein-protein interactions through mass spectrometry.[17,21,22,23] Endogenous fusion of AGO2 to HaloTag should therefore facilitate a thorough investigation of AGO2/RISC in human cells at physiologically relevant abundancies, in near-native cellular background, and to greater resolution than antibody-based approaches. Future HaloTag:AGO1-4 fusions would also enable comparative analysis of AGO1-4 biology in different contexts, with the mutual HaloTag overcoming the key limitations of CLIP-based methods that result from variable antibody performance.

Due to the stated versatility of HaloTag technology and advantages over traditional methods used to study AGO complexes and RISC, we aimed to create human cell lines endogenously expressing a new AGO2-HaloTag fusion protein to enable comprehensive study of AGO2 function and RISC biology in cells relevant to our research interests..

AGO2 comprises four domains (N-terminal (N), PIWI/Argonaute/Zwille (PAZ), middle (MID), and P-element-induced wimpy testes (PIWI)), each with known roles in RISC formation and RNA silencing.[24,25,26,27,28,29] When designing a recombinantly-tagged AGO2 protein, it is critical to consider the impact on both N- and C-terminal domains. The PIWI domain is located at the C-terminus of AGO2. This domain contains six loops along the nucleic acid-binding cleft and is similar in function to an RNase H domain, harbouring the catalytic triad (DDH) and catalytic tetrad (DEDH) essential for the slicing activity of AGO2.[29,30,31,32,33,34,35,36] Mutation of the conserved glutamate residue in the DEDH motif abolishes the ability of AGO2 to induce RNAi.[35] Many post-translational modifications (PTMs) of AGO2 are found in the C-terminal PIWI domain.[37] These PTMs impact various aspects of AGO2 function, ultimately influencing both RISC and miRNA activity. The C-terminal half of human AGO2 is also responsible for the interaction with TNRC6A, which is crucial for miRNA-dependent silencing function and the localization of AGO2 in cytoplasmic foci.[6] The N domain of AGO2 is fundamental to RISC functionality, facilitating ATP-independent unwinding of small RNA duplexes, a critical step for RISC assembly in human cells. Both slicer-dependent and slicer-independent unwinding require efficient function of the N domain of AGO2, highlighting its importance in passenger-strand cleavage. Moreover, two specific motifs (residues 44–48 and 134–166) in the N-terminal region of AGO2 are vital for optimal catalytic activity. It is postulated that, due to their proximity to the PIWI domain in the tertiary structure of AGO2, these motifs are essential for the accurate positioning of the guide-target. Alterations within these motifs hinder the activation of RISC and obstruct mRNA cleavage.[37,38,39] Deletions or mutations of the N-terminal lobe in *Drosophila* AGO2 resulted in decreased target RNA binding and constitutive activation of the cleavage activity of the PIWI domain.[40] These studies highlight the collective importance of both the N- and C-termini in the normal function of AGO2 and emphasise the need for consideration and due diligence when adding and validating tags at either terminus, as each may disrupt normal protein function.

Of relevance to this study, N-terminal fusion of HaloTag with Ago2 resulted in diminished ability to rescue RNAi in *Ago2*$^{-/-}$ MEFs compared to WT Ago2, de-repression of a subset of highly expressed miRNA targets, and reduced viability of *HaloTag-Ago2* homozygous mice,[14] indicating some loss of functionality due to the N-terminal HaloTag-Ago2 fusion. A series of functional validation experiments did, however, demonstrate core functionalities were retained after N-terminal HaloTag-Ago2 fusion. Pull-down assays established physical interaction between HaloTag-Ago2 and the core miRISC component Tnrc6a, while size-exclusion chromatography showed co-elution of HaloTag-Ago2 with WT Ago2 in high molecular weight complexes

(though, notably, complexes were of more variable size in tagged cells[9]). Encouragingly, Dual-Luciferase reporter experiments using three constructs with well-characterized miRNA binding sites, as well as a sensitive two-colour fluorescent reporter system,[41] showed no detectable differences in miRNA-mediated repression between *WT* and *Ago2*$^{Halo/Halo}$ MEFs. These findings are an example of orthodox tag validation and, overall, indicate endogenous N-terminal fusion of HaloTag to AGO(2) is a valuable model to study miRISC *in vivo* and *in vitro*. The tagging approach used by Li *et al*. raises important points of consideration when designing tags. N terminal fusion of HaloTag to Ago2 was achieved by insertion of a conditional knock-in allele containing the HaloTag upstream of a loxP-STOP-IRES-FLAG-loxP cassette in mouse ES cells to express Cre recombinase which fuses the HaloTag to the first exon of *Ago2*.[14] This is a relatively complex method of gene tagging which can be time-consuming and challenging to precisely reproduce. The approach also disrupts the 5′ UTR of the *Ago2* gene, risking unknown effects on the regulation of expression of AGO2, which is critical when considering true *in vivo* endogenous functionality. These challenges therefore prompted us to look for alternative methods to generate an endogenous HaloTag fusion to AGO2 in human cells.

CRISPaint is a gene editing system which allows the precise creation of C-terminal tag fusions of endogenously encoded proteins in human cells with high efficiency.[42] Unlike homology directed repair (HDR)-directed tagging, CRISPaint does not require generation of a site-specific donor template with homology arms but integrates heterologous genetic material via canonical non-homologous end joining (cNHEJ) in CRISPR-Cas9-accessible cellular systems. This reduces the overall time required to obtain genetically tagged cells compared with HDR-directed tagging.

The lack of data on the validity of C-terminal AGO2 tagging, the non-trivial nature of endogenous N-terminal AGO2 tagging, the importance of the 5′ UTR, and the critical motifs at both the C- and N-termini of AGO2 together make a preferred strategy for generating tagged variants of endogenous AGO2 tags challenging to predict. We therefore employed CRISPaint to create cell lines expressing a C-terminal AGO2-HaloTag fusion protein (AGO2^{HALO}) for the future comprehensive study of AGO2 in human cells. Due to the addition of the tag potentially impairing normal protein function and therefore invalidating any future results, as well as the lack of published evidence on the effect of C-terminal tagging of AGO2, we sought to validate the functional activity of endogenous AGO2^{HALO} robustly and diligently against native AGO2 in *UnTagged* CRISPaint controls lines and *WT* A549 cells.

By interrogating the core functional activities of AGO2 (protein localisation and binding, cleavage, and silencing capacity) in *WT, UnTagged,* and *AGO2*^{HALO} cells, we aimed to define the impact of the C-terminal fusion of AGO2 with HaloTag. Our results led us to conclude that *AGO2*^{HALO} cells have significantly impaired silencing function compared to control *UnTagged* and *WT* AGO2 cells, as well as distinct sub-cellular localisation. We therefore do not consider C-terminal AGO2^{HALO} as a suitable model for further study of AGO2 and RISC function. Although we only considered a single configuration for a single type of C-terminal fusion tag of the relatively large (33 kDa) HaloTag to AGO2, comparison of our data with previously published N-terminal HaloTag-AGO2 does indicate that N-terminal tagging is favourable.

Materials and Methods

Cell Culture

A549 cells were maintained in DMEM (Sigma, D8437) supplemented with 10% qualified fetal bovine serum (FBS) (Gibco, 10270106), 100 U/mL penicillin, and 100 µg/mL streptomycin (Gibco, 15140122) in a humidified 37 °C incubator and 5% CO_2. Cells were passaged every 3-4 days during the log phase of growth with Trypsin/EDTA solution (Gibco, R001100) following a PBS wash. To seed an exact number of cells, cell suspension concentration was counted using a Countess II™ Automated Cell Counter (Invitrogen). Parental stocks were obtained from ATCC. All cell cultures were regularly tested for mycoplasma. Post editing, isogenic lines (*A549 WT, UT C1, AGO2^{HALO} C5* and *AGO2^{HALO} C10*) were authenticated by STR profiling at 16 STR loci (***Sup Fig. 1***) using PCR-single-locus-technology (Eurofins Genomics).

CRISPaint Transfection and Puromycin Selection

The CRISPaint gene tagging kit was a gift from Veit Hornung (Addgene kit # 1000000086). To generate a targeting construct for AGO2, we used site-directed mutagenesis to change the gRNA sequence for TUBB to AGO2 gRNA sequence (AACATGTCAAGCAAAGTACA) in the pCas9 mCherry TUBB plasmid. For CRISPaint[42] transfection, A549 cells were plated in a 96 well plate and, per well, 50 ng pCas9 mCherry AGO2, 50 ng pCas9 mCherry Frame +1 and 100ng pCRISPaint HaloTag-Puro donor plasmids were transfected using ViaFect (Promega E498A). Three days post-transfection cells were sub-cultured into media supplemented with puromycin (0.8 µg/mL; Invivogen, ANT-PR-1). After six days of selection, cells were allowed to recover in media without puromycin for 12 days, followed by another round of puromycin selection for six days. After recovery, the cells were grown out in sufficient quantities to perform Western blotting of whole cell lysates of mixed populations. This was followed by single cell cloning in 96 well plates and once grown in sufficient quantities, individual clones were immunoblotted using the anti-HaloTag antibody (Promega) to screen for the AGO2-HaloTag fusion of approximately 130 kDa molecular weight. Two clones with no tagging of AGO2 (***UnTagged C1*** and ***UnTagged C2***) and two expressing AGO2-HaloTag (***AGO2^{HALO} C5*** and ***AGO2^{HALO} C10***) were selected for further evaluation in this study, alongside parental ***A549 WT*** cells. A schematic of the experimental design employed to generate and select *AGO2-HaloTag* (and non-transfected (*UnTagged*)) CRISPaint clones is provided in ***Fig. 1C***.

Genomic DNA Sequencing at AGO2-HaloTag Junction

Genomic DNA was prepared by removing the media and lysing the cells in 30 µl of gDNA lysis buffer (0.2 mg per mL proteinase K, 1 mM $CaCl_2$, 3 mM $MgCl_2$, 1 mM EDTA, 1% Triton X-100 and 10 mM Tris pH 7.5) and then incubating samples at 65 °C for 10 min and at 95 °C for 15 min. The *AGO2-HaloTag* junction region of this genomic DNA was amplified in a 25 µl Phusion Hot Start Flex (M05365S, NEB) PCR reaction as per the manufacturer's instructions, using specific forward (CAGCTGCTTTTCTGGAAGGG) and reverse (TCTTATGTACCTGACCGACG) primers. Following confirmation of correct PCR amplification on an 0.8% agarose Tris borate EDTA gel, PCR products were TOPO cloned using Zero Blunt™ TOPO™ PCR Cloning Kit for Sequencing (ThermoFisher K287520), transformed into 5-alpha Competent *E. coli* (C2987I, NEB) as per the manufacturer's protocol for plasmid preparation. Transformed colonies (≥ 5) were grown out in LB medium with 50 µg/mL Kanamycin and then pelleted before plasmids were isolated using the Monarch Plasmid Miniprep Kit (NEB, T1010L). Plasmids were sequenced (Sanger) from the T7 priming site of Blunt II-TOPO vector. Sequencing alignment was performed on BioEdit software.

Genomic DNA Primers	Sequence
AGO2 last intron FWD (Blue)	CAGCTGCTTTTCTGGAAGGG
AGO2 last exon REV (Blue)	CGTCTCATGTTCGATGCTGG
HaloTag FWD set 1 (Light Teal)	CCTGATCGGTATGGGCAAAT
HaloTag REV set 1 (Light Teal)	GGGCGGATGAACTCCATAA
HaloTag FWD set 2 (Dark Teal)	ACCAGACCTGGGTTATTTCTTC

HaloTag REV set 2 (Dark Teal)	GCAGCCAGTCCATGTATTCT

Analysis of Cell Doubling Time

Cell doubling time was measured using the IncuCyte ZOOM live-cell imaging platform (Essen Bioscience). Cells imaged using the IncuCyte were seeded in triplicate into 24 well plates at 12,000 cells per well and imaged at 10x magnification every 12 hours for 108 hours. Cell confluence per well was calculated using the IncuCyte ZOOM software (Essen Bioscience). Data represent mean ± SEM of three independent experimental repeats.

Western Blotting Analysis and Densitometry

Cells were lysed in RIPA buffer (150 nM NaCl, 1% (v/v) IGEPAL, 0.5% (w/v) deoxycholic acid, 0.1% (w/v) SDS, 50 mM Tris) supplemented with protease and phosphatase inhibitors (Pierce, Roche) during the log phase of growth. Protein concentration was quantified using the Pierce BCA protein assay kit (ThermoFisher Scientific, 23225). Lysates were electrophoresed on polyacrylamide gels transferred onto PVDF membranes and probed using the following antibodies: mouse anti-beta-Actin (Sigma #A1978), mouse anti-Vinculin (Invitrogen, 14-9777-82), rabbit anti-AGO1 (CST, 5053), rabbit anti-AGO2 (CST, 2897), rabbit anti-AGO4 (CST, 6913), mouse anti-HaloTag (Promega, G921A), rabbit anti-DDX6 (Bethyl, A300-460A), rabbit anti-GW182 (Bethyl, A302-329A) (TNRC6A), mouse anti-Dicer (Abcam, ab14601), mouse anti-alpha-Tubulin (GeneTex, GTX628802) and mouse anti-Histone H3 (Upstate, 05-499). Anti-IgG horseradish peroxidase (Dako) and chemiluminescent detection (ThermoFisher Scientific, Millipore WBKLS0500) were used to develop immunoblots. Blots were imaged on a GE Healthcare ImageQuant imager. Densitometry of immunoblot band intensity was performed on ImageJ, with target band intensity normalised to relative loading control intensity. Data represent mean ± SEM of three independent experimental repeats.

Protein Co-Immunoprecipitation

Cells from a 15 cm dish (one per elution) were lysed in 1 mL NP-40 buffer (150 mM NaCl, 50 mM Tris pH 8.0, 0.7% NP-40, 5% Glycerol) supplemented with protease and phosphatase inhibitors before centrifugation at 14,000 g for 5 minutes at 4 ºC to clear. After 80 µL of cleared lysate was taken for input and mixed with 20 µL of 5X Laemmli buffer and boiled for 5 minutes, cleared lysate (1 mL) was mixed with 1 µg of relevant antibody (Mouse IgA isotype control (eBioscience Invitrogen 14-4762-81) and Mouse IgA anti-AGO2 (Santa-Cruz, sc-53521) and rotated at room temperature for 3 hours. Protein L (Pierce, 88849) beads were washed twice in 500 µL of NP-40 buffer, resuspended in 30 µL of NP-40 buffer, and then added to each IP. Samples were conjugated by rotating for 1.5 hours at room temperature. Magnet bound samples were washed 4 times in 1 mL PBS with 0.1% Tween followed by elution of protein complexes by addition of 40 µL of 0.2 M Glycine (pH 2.5) and 3 minutes incubation at room temperature. Elutions were transferred to new tubes and neutralised with 5 µL of 1 M Tris-HCl (pH 8). Following addition of 11.25 µL of 5X Laemmli buffer and boiling for 5 minutes, samples were ready for analysis by western blot as described above.

Cell Fractionation

Nuclear and cytoplasmic cell fractions were prepared as performed previously.[43] Following lysis of cells with hypotonic lysis buffer, cells were incubated on ice for 10 minutes and centrifuged at 500 g for 5 minutes at 4 ºC. After supernatant was collected to form the cytoplasmic fraction, cell pellets were washed for three minutes in 0.5 mL of hypotonic buffer three times. Nuclear membrane was lysed with 0.5 mL of nuclear lysis buffer and sonicated for 20 seconds, followed by centrifugation at 15,000 g for 10 minutes at 4 ºC, with this supernatant forming the nuclear fraction. Samples were then prepared and analysed by Western blot as described above.

Luciferase Reporter Assays

To investigate endogenous silencing, two Renilla Luciferase reporter plasmids (one containing six *let-7a*-miR binding sites in its 3 UTR (CTCGAGAACTATACAACGTCTACCTCA; AACTATACAACGTCTACCTCA;

AACTATACAACGTCTACCTCAGTTTAAAC; AACTATACAACGTCTACCTCA; AACTATACAACGTCTACCTCA; AACTATACAACGTCTACCTCAGCGGCCGC)), and one containing empty vector ((V$_0$) psiCHECK2 (Promega, C8021)) were designed. Following cloning and verification by sequencing, plasmids were isolated using the Qiagen Midiprep kit and then diluted to 100 ng/µL in TE buffer for transfection.

Cells were plated in 24-well plates at 25,000 cells per well, and reverse transfected with 30 nM siRNA using DharmaFECT 1 Transfection Reagent (Horizon, T-2001,03) according to manufacturer's instructions (using Opti-MEM™ I (ThermoFisher Scientific, 11058021) and antibiotic free media). siRNA targeting hAGO2 (duplex sequence: 5′-3′ GGUCUAAAGGUGGAGAUA[dT][dT] and UUAUCUCCACCUUUAGACC[dT][dT]) and non-targeting control (scRNA (MISSION® siRNA Universal Negative Control #1, SIC001)) were both obtained from SIGMA and used to assess the impact of the tag on endogenous AGO2 silencing capacity. After 72 hours of incubation with siRNA, cells were transfected with 20 ng/well of psiCHECK-2 plasmid (psiCHECK-2 Vector (V$_0$) (Promega, C8021) or *let-7a*-mi6 targeting six regions of the 3′ UTR) using jetPRIME transfection reagent (Polyplus, 114-07) at 0.05 µL per well. Cells were lysed 26 hours later in 1 X Passive Lysis Buffer and stored at -80°C. After thawing, FireFly and Renilla Luciferase activities were measured using the Dual-Luciferase Reporter Assay System (Promega, E1960) according to the manufacturer's instructions on a FLUOstar® Omega microplate reader. Relative derepression was calculated by dividing normalised (to V$_0$) mean *let-7a*-mi6 reporter activity (Renilla luciferase activity/Firefly luciferase activity) in lysates from cells treated with si*AGO2* by normalised mean reporter activity in lysate from cells treated with scRNA.

For Firefly luciferase (FFLuc) silencing assays, cells were plated at 40,000 cells per well in 24 well plates. The following day cells were transfected using Attractene reagent (Qiagen, 301005) with pGL3 FFLuc, pGL4 RLuc (expressing Renilla luciferase for normalisation), and 60 ng/well of esiRNA targeting either GFP (control) (Sigma, EHUEGFP), or FFLuc (Sigma, EHUFLUC). After 48h, cells were harvested in 1X Passive Lysis Buffer and luciferase activities were assayed as above. Firefly luciferase activity was divided by the Renilla luciferase activity to normalise the data.

MiR-451 RT-qPCR

TRIzol reagent (Invitrogen, 15596026) was used to isolate total RNA from cells at indicated confluency (log-phase = ~60% confluency; confluent = ~95% confluency) 60 hours after plating according to the manufacturer's instructions (with an additional 70% ethanol wash of RNA pellets). cDNA was generated from total RNA using the miRCURY LNA RT Kit (QIAGEN, 339340) and then amplified in duplicate by qPCR using the miRCURY LNA SYBR Green PCR Kit (QIAGEN, 339345) on a QuantStudio™ 5 Real-Time PCR machine (Applied Biosystems) with primers targeting *miR-451a* (QIAGEN, 3624799) and *U6* snRNA (v2) (QIAGEN, 3608295). *MiR-451a* CT values were normalized to *U6* and relative (to relevant WT) fold transcript abundance was calculated using the $2^{-\Delta\Delta Ct}$ method. Data represent mean ± SEM of two independent experimental repeats.

AGO2 WT RT-qPCR

To assay for untagged *AGO2* mRNA in our cells, total RNA was first extracted using TRIzol reagent according to the manufacturer's instructions. 1 µg of RNA was treated with amplification grade DNase I (Sigma) for 15 min at room temperature, followed by inactivation of DNase I by addition of stop solution and incubation at 70 °C for 10 min. A six-point serial dilution was prepared of RNA for generation of standard curves. Diluted RNA was assayed for *AGO2* transcript using the GoTaq 1-Step RT-qPCR System (Promega A6020) with primers CTGGCTCCAGGGGACAAG (Forward primer) and CCACTCGGTACACAATCGCT (Reverse primer). *Beta Actin* mRNA was also assayed as a housekeeping gene (using primers CTGGAACGGTGAAGGTGACG (Forward primer) and AAGGGACTTCCTGTAACAATGCA (Reverse primer)) to normalise AGO2 transcript abundance. Primers were purchased from Integrated DNA Technologies.

Immunocytochemistry and HaloTag Labelling

Small round 1.5 coverslips were coated with Poly-L-Lysine (P4707) as per the manufacturer's instructions. Cell culture mix (0.5 mL) was added to wells containing coated coverslips and left 48 hours for cells to settle before fixation in 4% paraformaldehyde and immunostaining overnight with mouse anti-AGO2 mAb (Sigma Aldrich 04-642 clone 9E8.2) or rat anti-AGO2 mAb (Millipore MABE253 clone, 11A9) diluted in 2% bovine serum albumin in PBS. After washing away excess primary antibodies, coverslips were incubated for 1 h with Alexa Fluor (AF)-conjugated secondary antibodies; anti-mouse AF568 (A11031), anti-rat AF546 (A11081). Following brief immersion of coverslips in distilled water to remove excess salts, coverslips were mounted onto a drop of mounting media containing DAPI (EverBrite™ Hardset Mounting Medium, biotium (#23004)) on glass slides, and cured in the dark overnight in preparation for imaging by microscopy. For cells which underwent covalent protein labelling with HaloTag-TMR, prior to fixation HaloTag® TMRDirect^{TM} Ligand (Promega, G2991) was added to cell culture medium to a concentration of 100 nM and incubated overnight. Cells were washed three times in fresh cell culture medium and incubated for 30 minutes before a final wash, fixation, and then immunostaining with antibodies. Slides were imaged with the ZEISS LSM 880 with Airyscan confocal microscope (64 X oil objective). Signal gain and offset were optimised for each experiment, set against a comparable negative control sample. Images were processed using ZEN 3.4 (blue edition) (Zeiss). Nuclear and cytoplasmic signal intensities (per cell) were quantified using ImageJ.

Structural Analysis

Atomic resolution structures of AGO2 were accessed via RCSB (https://www.rcsb.org). AlphaFold[44] predictions of full-length AGO2 were taken from the DeepMind-EBI database (https://alphafold.ebi.ac.uk; Access date: 08/2023). The structure of AGO2^{HALO} was predicted using ColabFold v1.5.3.[45] Solvent accessible surfaces areas of AGO2 (PDB accession code, 4OLB) were calculated using the POPScomp server (http://popscomp.org:3838/) using a solvent radius of 1.4 Å.[46] Figures were made using PyMol (Schrodinger).

Statistical Analysis

Statistical significance was calculated using the Student's t-test using GraphPad Prism 9.5.0 and is represented as: not significant (ns) > 0.05; *p ≤ 0.05; **p ≤ 0.01; ***p ≤ 0.001 throughout. Data and error bars represent mean ± SEM of three independent experimental repeats, unless otherwise stated. Technical replicates (≥ 2) were performed in each independent experimental repeat for each sample and condition where possible.

Results

Creation and Genomic Characterisation of *AGO2*^{HALO} Cell Lines

To investigate the functional activity of AGO2 fused at the C-terminus to HaloTag, we first generated *AGO2*^{HALO} cells using CRISPaint technology (***Fig. 1A***). Following CRISPaint transfection of A549 cells, successful editing should result in the insertion of HaloTag sequence (as well as sequence for a T2A site, Puromycin Resistance, and Poly(A) Tail) to the last exon of the endogenous *AGO2* locus (***Fig. 1B***). After transfection, puromycin selection, and initial screening to confirm successful editing to fuse *AGO2* with *HaloTag*, two untagged control (*UnTagged C1* (***UT C1***) and *UnTagged C2* (***UT C2***)) and two *AGO2*^{HALO} (***AGO2***^{HALO} ***C5*** *and* ***AGO2***^{HALO} ***C10***)) clonal cell populations were selected for further evaluation in this study alongside parental ***A549 WT*** cells (***Fig. 1C***). By selecting two *AGO2*^{HALO} and two *UnTagged* CRISPaint control lines to compare against each other and to *WT* A549 cells we hoped to accord greater confidence when interpreting results.

Amplification of genomic DNA (gDNA) revealed that, as expected, HaloTag sequence was only present in *AGO2*^{HALO} clones (***Fig. 1D***). Sequencing of *AGO2*^{HALO} *C5* and *C10* cell populations identified two *AGO2*^{HALO} variants, one long and one short (***Fig. 1E***). Mutations in the long variant replaced the final two amino acids of AGO2 (FA) before the STOP codon of the *AGO2* sequence, while the shorter variant had lost six amino acids (RTMYFA) before the Linker and *HaloTag* sequences. The two pairs of long and short variant sequences are identical in both *AGO2*^{HALO} clones. Neither tagged variant results in loss of any PIWI domain loops or motifs known to harbour direct functional importance (***Fig. 1F***).[36,37,47]

Curiously, we observed amplification of *WT AGO2* sequence at the *AGO2-HaloTag* junction in both *AGO2*^{HALO} clones (***Fig. 1D***), indicating retention of non-HaloTagged *AGO2* gDNA in edited *AGO2*^{HALO} cells. Sequence alignments of these products identified an additional premature STOP codon (TAA) in both *AGO2*^{HALO} clones (***Fig. 1G***). This slightly truncated *AGO2* sequence resulted in appreciable levels of non-HaloTagged *AGO2* mRNA transcript in both *AGO2*^{HALO} clones (~40% of normalised *WT AGO2* mRNA abundance in *A549 WT* cells) (***Fig. 1H***). Crucially, however, we did not observe any of this truncated AGO2 during protein analysis of the lines by immunoblot (even at long exposures and adjusted intensities) (***Fig. 1I***), suggesting the premature STOP codon results in very efficient nonsense-mediated mRNA decay (NMD) of this transcript before translation.[48] Correspondingly, immunoblot with anti-AGO2 and anti-HaloTag antibody showed a band in the *AGO2*^{HALO} lines at 130 kDa, the correct predicted size for a fusion protein of AGO2 (97 kDa) and HaloTag (33 kDa), (***Fig. 1I***), confirming the HaloTag was fused with AGO2 in-frame and translated correctly.

Characterisation of Growth Rate and RISC Abundance in *AGO2*^{HALO} Cells

As AGO2 is essential for many cell functions, we first probed whether C-terminal *AGO2*^{HALO} resulted in changes to cell proliferation. The observed mean doubling time in *WT* cells of 26.5 ± 2.6 h was broadly similar to that in both *UnTagged* (*UT C1* = 26.4 ± 0.8 h; *UT C2* = 30.6 ± 2.8 h) and *AGO2*^{HALO} cells (*AGO2*^{HALO} *C5* = 28.4 ± 1.9 h; *AGO2*^{HALO} *C10* = 27.6 ± 1.8 h), with no statistically significant differences observed and the greatest change (in relation to *WT*) detected in *UT C1* cells (***Fig. 2A***). These data suggest *AGO2*^{HALO} fusion does not cause a discernible difference in cell proliferation rates, and that clonal selection has greater potential than *AGO2*^{HALO} fusion to influence cell proliferation rate.

Due to potential compensatory effects arising from impaired AGO2 function in *AGO2*^{HALO} cells, we considered whether the *AGO2*^{HALO} fusion resulted in changes to alternative and partner RISC protein abundance. Densitometry of immunoblots probed for key RISC proteins showed that both *AGO2*^{HALO} clones continued to express other Argonaute family members (AGO1/3/4) and the core RISC proteins TNRC6A, DDX6, and LIMD1 (***Fig. 2B-E***). Although abundance of TNRC6A, DDX6, and LIMD1 remained stable across lines, we did note increased AGO1 (not statistically significant) and AGO4 abundance (statistically significant rise from *WT* and *UT C1* to *AGO2*^{HALO} *C5* and *C10*) in *AGO2*^{HALO} cells compared with *WT* and *UnTagged* cells. This could be due to compensation/functional buffering occurring in *AGO2*^{HALO} cells to counter impaired AGO2 function.[49] We also observed a decrease in AGO2 abundance in both *AGO2*^{HALO} lines compared with *WT* and *UT C2*, but not *UT C1*,

cells. As significant changes in protein abundance were also observed in *UnTagged* clones compared to *WT*, we were unable to conclude if these decreases were caused directly by *AGO2*^{HALO} fusion or clonal selection. Nevertheless, the continued expression of these RISC proteins within a level of variation which is likely tolerable for investigation of the basic biology of AGO2 and RISC in translational control encouraged us to continue to validate and define the functionality of *AGO2*^{HALO} cells.

AGO2^{HALO} Shows Comparable Binding to TNRC6A and Increased Binding to Dicer

A core function of AGO2 is to bind other proteins involved in RNA processing and silencing to form a complex to regulate translational control.[2,6] We explored whether AGO2^{HALO} can bind TNRC6A - a key protein involved in miRNA-mediated silencing which acts to form a functional RISC when complexed with AGO2[6] - and Dicer - a critical miRNA processing protein which cleaves precursor miRNAs to generate mature miRNAs and which can also act as a platform for RISC assembly when complexed with AGO2.[50] Endogenous co-immunoprecipitation of AGO2 with TNRC6A in *WT*, *UnTagged* and *AGO2*^{HALO} cells showed AGO2^{HALO} associating with TNRC6A comparably in *UnTagged* (*C2*) and *AGO2*^{HALO} (*C10*) cells (***Fig. 3A***). The similar binding of these two core RISC proteins indicates that the RISC can assemble in *AGO2*^{HALO} cells. When examining AGO2:Dicer association we observed a greater co-immunoprecipitation of Dicer with AGO2 in *AGO2*^{HALO} cells than in *WT* and *UnTagged* cells (***Fig. 3A-B***), suggesting some modified AGO2 activity in *AGO2*^{HALO} cells.

Fusion of *AGO2*^{HALO} Impairs AGO2 Cleavage and Silencing Capacity

The pre-eminent function of AGO2 in an active RISC is to correctly and efficiently pair miRNAs with their targets to regulate mRNA translation. This can occur by direct cleavage of the mRNA by AGO2 after small RNA:mRNA binding (with perfect complementarity) or, where (partial or full) seed matching is achieved, through a variety of alternative mechanisms which include recruitment of CCR4-NOT, eIF4F inhibition, ribosome blocking, and mRNA decapping.[2] To interrogate if *AGO2*^{HALO} fusion affected AGO2 cleavage function, we measured *miR-451a* abundance in our cells. Unlike most miRNAs, maturation of the highly conserved vertebrate *miR-451* bypasses Dicer, instead requiring direct cleavage of its precursor hairpin through catalytic AGO2 slicer activity.[51,52,53,54] Due to this strict AGO2 slicer dependency, the presence of mature *miR-451a* in the cell demonstrates AGO2 catalytic function activity. We used RT-qPCR to quantify the normalized abundance of *miR-451a* in *WT*, *UnTagged*, and *AGO2*^{HALO} cells (***Fig. 4A***). Cells were assayed during the log-phase and near confluency due to the known association of increased cell density with miRNA abundance, miRNA processing, efficiency of RISC formation and RISC composition.[13,55] We observed comparable normalized *miR-451a* abundance in *WT* (1.00 ± 0.00) and *AGO2*^{HALO} cells (*AGO2*^{HALO} *C5* = 1.16 ± 0.01; *AGO2*^{HALO} *C10* = 0.79 ± 0.11) during the log-phase of growth. However, due to the observed increase (relative to *WT*) of *miR-451a* abundance in both *UnTagged* clones (*UT C1* = 1.91 ± 0.23; *UT C2* = 2.59 ± 0.49), there was a notable reduction of normalised *miR-451a* abundance in *AGO2*^{HALO} cells relative to *UnTagged* control cells during the log-phase (*AGO2*^{HALO} *C5* vs *UT C1* = 0.6-fold, p=0.086; *AGO2*^{HALO} *C5* vs *UT C2* = 0.4-fold, p=0.102; *AGO2*^{HALO} *C10* vs *UT C1* = 0.4-fold, p=0.051; *AGO2*^{HALO} *C10* vs *UT C2* = 0.3-fold, p=0.072).

In cells assayed near confluency, normalised *miR-451a* abundance compared with *WT* (1.00 ± 0.00) was markedly reduced in both *AGO2*^{HALO} lines (*AGO2*^{HALO} *C5* = 0.32 ± 0.12; *AGO2*^{HALO} *C10* = 0.38 ± 0.01), while mean abundance in both *UnTagged* lines increased (*UT C1* = 1.29 ± 0.36; *UT C2* = 1.37 ± 0.02). Compared to *UnTagged* cells, *AGO2*^{HALO} cells had significantly lower *miR-451a* abundance at confluency (*AGO2*^{HALO} *C5* vs *UT C1* = 0.2-fold, p=0.121; *AGO2*^{HALO} *C5* vs *UT C2* = 0.2-fold, p=0.013; *AGO2*^{HALO} *C10* vs *UT C1* = 0.3-fold, p=0.123; *AGO2*^{HALO} *C10* vs *UT C2* = 0.3-fold, p=0.0005).

Despite the presence of *miR-451a* in all conditions implying some degree of AGO2 cleavage function capacity is maintained in *AGO2*^{HALO} cells, the observed reduction in *miR-451a* abundance compared with *UnTagged* control cells, particularly when cells were near confluency, suggests C-terminal *AGO2*^{HALO} fusion resulted in significantly impaired *miR-451a* biogenesis and therefore AGO2 catalytic activity.

As measures of *miR-451a* abundance constitute only a qualified test for AGO2 cleavage function, we also used two different types of Dual-Luciferase reporter assays to further investigate if C-terminal fusion of *AGO2*^{HALO} impairs endogenous silencing capacity of AGO2, critical for functionality. For investigation of endogenous silencing capacity, we designed a Renilla Luciferase reporter containing six *let-7a* binding sites in its 3′ UTR, or an empty vector (lacking miRNA binding sites) and compared the ratio of normalized Renilla Luciferase activity in cells treated with siRNA targeting h*AGO2* against those treated with non-targeting control (scRNA). Strikingly, we observed significant derepression of the *let-7a-mi*6 reporter upon *AGO2* siRNA-mediated knockdown in *WT* (1.34 ± 0.08 fold, p=0.040) and *UT C1* (1.56 ± 0.09 fold, p=0.004) cells, but not in *AGO2*^{HALO} *C10* cells (0.94 ± 0.07, p=0.721) (***Fig. 4B***). Subsequently, we also used the Dual-Luciferase reporter system to measure activity ratios after co-transfection of exogenous Luciferase reporter plasmids (Firefly and Renilla Luciferases) in cells treated with esi*GFP* and esi*FFLuc* (***Fig. 4C***). Here we observed significant repression (~80%) of the FFLuc reporter upon esiFFLuc transfection in *WT* (p=0.007) and *UT C1* (p=0.001) cells, but negligible repression in *AGO2*^{HALO} *C5* (p=0.462) and, though statistically significant, a markedly reduced (~30%) level of repression in *AGO2*^{HALO} *C10* (p=0.001) cells. Together, these data indicate that C-terminal *AGO2*^{HALO} fusion results in significant impairment to endogenous AGO2-dependent silencing and cleavage function.

AGO2^{HALO} Fusion Results in Impaired Nuclear Localisation Compared to AGO2 in *WT* and *UnTagged* Cells

As mRNA translation is regulated temporally and spatially, correct sub-cellular localization of AGO2 and RISC is crucial for normal function. We used microscopy and cell fractionation experiments to investigate if the fusion of HaloTag to the C-terminus of AGO2 altered its sub-cellular localization. *AGO2*^{HALO} cells treated with TMRDirect Ligand (HaloTag specific ligand) showed a predominantly cytoplasmic signal (***Fig. 5A***). Intriguingly, we observed that AGO2 (and *AGO2*^{HALO}) probed with Mouse anti-AGO2 (clone 9E8.2) antibody had a conspicuously greater nuclear signal than AGO2, and *AGO2*^{HALO}, probed with Rat anti-AGO2 antibody (clone 11A9) (***Fig. 5B***). This difference in Mouse and Rat anti-AGO2 signal notably existed in both *UT C1* (mean Mouse anti-AGO2 nuclear:cytoplasmic ratio = 2.8 ± 0.5 SD; mean Rat anti-AGO2 nuclear:cytoplasmic ratio = 0.4 ± 0.1 SD, p=0.018) and *AGO2*^{HALO} *C10* (mean Mouse anti-AGO2 nuclear:cytoplasmic ratio = 1.5 ± 0.3 SD; mean Rat anti-AGO2 nuclear:cytoplasmic ratio = 0.9 ± 0.2 SD, p=0.057) cells (***Fig. 5C***). Comparison of the nuclear:cytoplasmic ratio of AGO2 in *UT C1* and *AGO2*^{HALO} *C10* cells using both antibodies yielded contradictory results. When probing with Mouse anti-AGO2, the nuclear:cytoplasmic ratio in *AGO2*^{HALO} *C10* cells was approximately 0.5-fold lower than in *UT C1* cells (p=0.018), but when probed with the Rat anti-AGO2 the ratio in *AGO2*^{HALO} *C10* cells was approximately 2-fold higher than in *UT C1* cells (p=0.021). These conflicting findings complicate the interpretation of the immunofluorescence images, limiting our ability to definitively assess the effect of *AGO2*^{HALO} fusion on the sub-cellular localization of AGO2. Notably, the TMRDirect-HaloTag signal in *AGO2*^{HALO} *C10* cells (mean TMRDirect-HaloTag nuclear:cytoplasmic ratio = 0.5 ± 0.1 SD) displayed greater visual similarity to the Rat anti-AGO2 signal (p=0.046) than the Mouse anti-AGO2 signal (p=0.018), and a nuclear:cytoplasmic ratio below 1. As the TMRDirect-HaloTag signal is anticipated to be highly specific to HaloTag, which when conjugated to AGO2 shows a stronger cytoplasmic than nuclear signal, the strong and incongruent nuclear signal observed in *AGO2*^{HALO} *C10* cells probed with mouse anti-AGO2 indicates the rat anti-AGO2 antibody signal may be a more accurate marker of AGO2 localisation than the Mouse anti-AGO2 antibody.

To further investigate and clarify the sub-cellular localization of the AGO2 fusion protein in *AGO2*^{HALO} cells compared with AGO2 in *WT* and *UnTagged* cells, we performed nuclear and cytoplasmic fractionation (***Fig. 5D***). Our results show that there is much weaker (almost undetectable at normal exposures) nuclear AGO2 signal in *AGO2*^{HALO} cells compared with *WT* and *UnTagged* clones. Correspondingly, a clear signal for HaloTag was observed in cytoplasmic fractions of *AGO2*^{HALO} cells, but not in the nuclear fraction of these cells. Given the rat anti-AGO2 antibody displayed little nuclear signal in *AGO2*^{HALO} and *UnTagged* cells and the mouse anti-AGO2 the opposite (strong nuclear signal in both), it remains unclear which of these antibodies, if any, is a valid indicator of AGO2 localisation when considering this fractionation data. Nevertheless, this fractionation data established AGO2 protein localisation in *AGO2*^{HALO} cells as markedly distinct to that of *WT* and *UnTagged*

cells, re-enforcing that C-terminal *AGO2*^{HALO} fusion disrupts normal AGO2 function. When coupled with findings indicating impaired silencing function described above, this altered sub-cellular localisation led us to ultimately conclude that C-terminal *AGO2*^{HALO} fusion was not a suitable model for further study of the basic biology of AGO2 and RISC.

When comparing whole cell lysate to nuclear and cytoplasmic fractions (***Fig. 5D***), we deduced that the fractionation method (speculatively, either the buffers used for lysis or addition of a sonication step), intensified observable AGO2 signal. This AGO enrichment enabled us to here observe detectable levels of unedited (*WT*: 97 kDa) AGO2 in the cytoplasmic fraction of *AGO2*^{HALO} *C5* and *C10* cells which, even when loading high protein amounts and adjusting images for high contrast, had been undetectable in our previous AGO2 Western Blots of whole cell lysate. The detection of this residual amount of AGO2 at the unedited molecular weight of 97 kDa presumably results from incomplete NMD of the afore described *WT AGO2* mRNA transcript present in *AGO2*^{HALO} *C5* and *C10* cells.

Discussion

CRISPaint Generated *AGO2*^{HALO} Cells have Comparable miRISC Core Protein Component Abundancies and Cell Viability as *WT*.

We successfully used CRISPaint technology to introduce a C-terminal *HaloTag* to *AGO2* to create *AGO2*^{HALO} cells (***Fig. 1***). Two identical variants were identified in both *AGO2*^{HALO} clones, suggesting selectivity for these two specific fusion events. We note that the specific sequence outcomes of fusion events are hard to predict due to the potential for bases to be lost during repair. If precise fusion occurs, the CRISPaint-*AGO2* targeting gRNA we employed would fuse AGO2 with a C-terminal HaloTag with loss of the three C-terminal amino acid residues of AGO2. WT human AGO2 is 859 residues long. However, we identified two unique variants: "long", 857 residues; and "short", 853 residues.

Unexpectedly, we detected a non-HaloTagged AGO2 sequence (covering the gene-tag (*AGO2-HaloTag*) junction) and appreciable levels of *WT AGO2* mRNA transcript in both *AGO2*^{HALO} clones. The absence of observable non-HaloTagged AGO2 in *AGO2*^{HALO} cells by immunoblot, even at long exposures and high input amounts, initially led us to conclude that these transcripts undergo efficient NMD, presumably because of the two premature STOP codons.[48] However, we did not rule out that some of this non-HaloTagged *AGO2* transcript may be translated into truncated AGO2 protein, even if only stable for a short period. This was indeed observed later in our study, where we detected ~97 kDa AGO2 signal in our *AGO2*^{HALO} lines by immunoblot when loading fractionated protein lysate, a process which seems to enrich or concentrate the AGO protein signal (***Fig. 5C***). NMD has been shown to have a broad range of efficiency in cell populations, with some cells degrading essentially all mRNAs while others escaped NMD completely.[56] It remains plausible that, due to the importance of functional AGO2 in the cell, there is survival selection for *AGO2*^{HALO} CRISPaint clones which have less efficient NMD and therefore continue to express (possibly at very low levels) WT (truncated) AGO2 protein. However, this argument is somewhat clouded due to the known role of AGO2/RISC as an inhibitory regulator of NMD itself.[57,58]

Despite the retained expression of very low levels of non-HaloTagged AGO2 in *AGO2*^{HALO} lines, we concluded from our immunoblots that the abundance of non-HaloTagged AGO2 protein in *AGO2*^{HALO} was so low in comparison to the levels of AGO2 seen in *WT* and *UnTagged* cells that it would quickly become saturated. Therefore, this truncated AGO2 would have minimal impact on silencing in the cell and so our experiments evaluating silencing function in *AGO2*^{HALO} cells remain valid - especially given that we observed disruption to, rather than retention of, function. The different variants and editing events described herein likely reflect the specific hypotriploid karyotype of A549 cells,[59] the challenge of creating multiple 'identical' edits of AGO2 in this complex and highly mutated genomic context, and the need for researchers to comprehensively define their tag-editing at the DNA, RNA, and protein level.

Having validated the successful generation of *AGO2*^{HALO} fusion cells, we next sought to define the basic characteristics of the cell. Due to the central nature of AGO2 in normal cell function, tagging of AGO2 may have resulted in differential proliferation. Indeed, down-regulation of *AGO2* has been associated with cell proliferation and apoptosis in prostate cancer.[60] Encouragingly, our data indicated little change in cell proliferation, with clonal selection potentially having a greater influence on proliferation than *AGO2*^{HALO} fusion (***Fig. 2A***).

The first indication that C-terminal fusion of *AGO2*^{HALO} caused impairment to normal function was noted from the observed increase in abundance of AGO1 and AGO4 in *AGO2*^{HALO} lines compared with *WT* and *UnTagged* cells. This may be due to 'compensation' between Argonaute proteins following defective AGO2 activity. It has been proposed that there is a degree of functional redundancy between Argonaute proteins, where ablation or silencing of one Argonaute can be 'compensated' by other Argonaute proteins.[3] For example, *AGO2* knock-out can result in increased AGO1 abundance, and vice versa, and AGO3 levels were shown to increase in *AGO1*, *AGO2*, or *AGO1+AGO2* knock-out cells: generally, *AGO* knock-out results in increased abundance of the remaining AGO proteins to maintain overall AGO expression at a level near that of *WT*.[49] If *AGO2*^{HALO} fusion were to impair normal AGO2 function, the observed increase in AGO1/4 abundance (***Fig. 2B-C***) would be explained by a need to compensate for the reduced (AGO2) silencing capacity in *AGO2*^{HALO} cells. We also considered that some changes may simply be caused by clonal selection, highlighted by the significant reduction in AGO2 abundance in *UT C1* cells. Despite these differences, the variations observed were appreciable but not alarming and, together with the retained abundance of RISC proteins which partner with AGO2 during translational regulation (DDX6, TNRC6A, and LIMD1) (***Fig. 2D-E***), implied *AGO2*^{HALO} cells have tolerable RISC activity and encouraged us continue with more direct and quantifiable experimental work to validate *AGO2*^{HALO} functionality as a suitable model for study of RISC .

AGO2^{HALO} Cells Retain TNRC6A Binding Capacity, but Differential Dicer Binding Suggests Abnormal Functionality

We showed that AGO2^{HALO} fusion protein can bind TNRC6A to a similar level as native AGO2 in *WT* and *UnTagged* cells (***Fig. 3A***). As TNRC6A is a critical binding partner of AGO2 - with binding normally necessary for assembly of a functional RISC[2,6] - this interaction supports that, like the N-terminal HaloTag-Ago2 fusion protein,[14] the C-terminal AGO2^{HALO} fusion protein can form an operative RISC with TNRC6A. Indeed, as TNRC6A interacts with AGO2 via three tryptophan binding pockets in the PIWI domain that bind optimally spaced Trp residues in TNRC6A Motfis I, II and Hook, the observed interaction with TNRC6A suggests that AGO2^{HALO} has a correctly folded PIWI domain, and that AGO2 is likely correctly folded overall.[61,62] However, the increased association of AGO2 with Dicer in *AGO2*^{HALO} cells (***Fig. 3A-B)*** indicated *AGO2*^{HALO} fusion caused impairment of normal protein activity. Dicer is critical for miRNA processing, cleaving precursor miRNAs to generate mature miRNAs, and can also act as a platform for RISC assembly with AGO2 (and TRBP).[50] One plausible cause of increased AGO2:Dicer association in *AGO2*^{HALO} cells would be a deterioration in miRNA-mediated translational repression as a result of impairment to normal function. Speculatively, this might ultimately lead to accumulation of AGO2:Dicer containing complexes to process more miRNAs and form more active RISCs to compensate for the impaired function. Alternatively, the increase in AGO2:Dicer complex levels could suggest that the addition of a C-terminal HaloTag to AGO2 might stabilise the RISC-loading complex and impair the necessary downstream subunit exchange steps.[50] It would be interesting to determine whether *AGO2*^{HALO} constructs also associate with TRBP. Nevertheless, we would expect any tag-fusion to result in some changes to normal AGO2 function and, most importantly, data thus far supported a functional RISC could assemble in *AGO2*^{HALO} cells.

AGO2^{HALO} Cells Have Significantly Impaired Cleavage and Silencing Function

Ultimately, for C-terminal *AGO2*^{HALO} cells to act as a valuable platform to study AGO2 and RISC, data must support that the key protein activities of slicing and miRNA-mediated silencing are sufficiently retained. As such, we focussed on efficiently demonstrating and quantifying catalytic slicing (measuring *miR-451a*

abundance) and *let-7* miRNA mediated silencing (measuring derepression of endogenous Luciferase miRNA reporter targets and exogenous silencing) functionality in *AGO2*^{HALO} cells (***Fig. 4A-C***).

Although the presence of mature *miR-451a* (strict AGO2 slicer dependency) indicates some slicing function in *AGO2*^{HALO} cells, the significantly reduced (compared to *UnTagged* cells) *miR-451a* abundance in *AGO2*^{HALO} cells suggests there is consequential deterioration in AGO2 slicing ability arising from *AGO2*^{HALO} fusion. It remains unclear precisely why *miR-451a* is less abundant in *AGO2*^{HALO} than *WT* cells at confluency but not during the log-phase. However, it has previously been shown that RISC composition, efficiency of RISC formation, RISC activity, miRNA processing, and miRNA abundance are all cell density dependent.[13,55,63] This leaves open the possibility that certain experimental conditions encompass specific windows of AGO expression, or specific cellular and/or RISC contexts, which are less detrimental to AGO2^{HALO} functionality, helping to explain why different *miR-451a* relative abundance was observed at different cell densities.

Given the convenient but narrow use of *miR-451a* abundance as a measure of AGO2 slicing function, we next sought to quantify endogenous AGO2 silencing capacity in *AGO2*^{HALO} cells using Dual-Luciferase reporter assays. Our results showed a failure of (fusion-tagged) AGO2 in *AGO2*^{HALO} cells to repress a *let-7a*-targeted miRNA reporter, and poor repression of transfected FFLuc compared to that achieved in *WT* and *UnTagged* cells (***Fig. 4B-C***). Together, these data strongly indicate that the core function of AGO2 in cells is impaired due to the *AGO2-HaloTag* fusion.

Comparison of our reporter data with previously published evidence of the effect of N-terminal *HaloTag-Ago2* fusion in MEFs indicates that C-terminal *AGO2*^{HALO} fusion in A549 cells results in greater impairment to silencing function. Dual-Luciferase reporter experiments which were related, but not interchangeable, to ours did not show measurable differences in repression between *WT* and *Ago2*$^{Halo/Halo}$ MEFs for three miRNA binding site containing constructs (*PTEN* 3′ UTR *miR-29* binding site; *Adrb2* 3′ UTR *let-7* binding site; *Taf7* 3′ UTR *miR-21* binding site), though these experiments did not knock-down or perturb Ago2 and so specific Ago2 and HaloTag-Ago2 activity may not have been assessed.[14] These findings were re-affirmed by a sensitive two-colour fluorescent reporter system.[14] Notably, however, the N-terminal *HaloTag-Ago2* fusion did result in slight preferential derepression of miRNA targets, reduced viability of homozygous mice, and reduced ability to rescue RNAi in *Ago2*$^{-/-}$ MEFs compared with WT Ago2.[14]

Notwithstanding, in both comparative and absolute terms our data led us to conclude that C-terminally fused *AGO2*^{HALO} cells have significantly impaired endogenous AGO2-mediated silencing function compared to *WT* and *UnTagged* cells. This evidence of such impairment to AGO2 silencing caused by C-terminal fusion of *AGO2*^{HALO} does not support *AGO2*^{HALO} as a suitable model for the study of AGO2 and RISC biology. Regarding the validation of tagged AGO2, we urge for increased use of orthogonal standardised and reproducible (where possible) experimental measures of AGO2 silencing capacity. We believe this will ensure comparability between studies (and tags/tagging strategies), as well as ultimately save researchers valuable time and resources.

A Molecular Explanation for Impairment of AGO2 by Addition of a C-terminal HaloTag

Inspection of the 3D structure of human AGO2[50,61] provides insight as to why a C-terminal HaloTag impairs activity. Protein termini are typically solvent exposed,[64] however, the C-terminus of AGO2 is an uncommon example where the last residue is buried (only 20% of the surface area of A859 is accessible to a solvent probe with radius 1.4 Å). The buried carboxylate group of A859 also forms functionally relevant interactions (Fig. 6A), including hydrogen bonds with several residues (e.g. K556 and R792) that themselves interact with the phosphate groups of residues 1 and 3 of the miRNA. Moreover, in some of the reported structures, the carboxylate groups of Y857 and A859 interact with a buried water molecule that also interacts with the 5′ terminal phosphate group of the miRNA. Evidently, modification of the sequence in this region of the protein via deletion of native residues and addition of a HaloTag will likely perturb the RNA binding properties of AGO2 (Fig. 6B). Indeed, prediction of the AGO2^{HALO} structure using AlphaFold2 shows the linker region between

AGO2 and the HaloTag exiting AGO2 via the miRNA binding site (data not shown). While the confidence (both pLDDT and PAE) for this region of the model is low, this prediction is consistent with our experimental data.

By contrast, the N-terminus of AGO2 is solvent exposed (Fig. 6C), which is consistent with previously reported successful tagging of this end of the protein for both *in vitro* and in cell studies. Indeed, crystal structures of AGO2 tend to lack data for the first 20-25 residues,[50,61] presumably due to the inherent flexibility of this region. Prediction of the structure of full-length AGO2 using AlphaFold2[44] shows low confidence for the first 25 residues, consistent with them being flexible and solvent-exposed.[65]

Our data on *AGO2*^{HALO} are interesting in that not all function is impaired. Both short and long constructs remove residues from the native sequence, while both add a linker and the HaloTag sequence (Fig. 1E). Given what is known about the location and role of the AGO2 C-terminus, it could have been expected that both constructs would disrupt protein folding. However, only slicing activity was impaired; binding to Dicer and TNRC6A is retained (***Fig. 3A-B***), which suggests that the surfaces of AGO2 required for these interactions remain functional.

The interaction between AGO2 and TNRC6A is well-characterised. Conserved tryptophan residues in TNRC6A interact via three optimally spaced binding pockets in the PIWI domain of AGO2 (Fig. 6C).[62,61] Each site binds the Trp indole ring with low affinity and thus efficient binding of TNRC6A is contingent on all sites being present and functional, which would require correct folding of the PIWI domain. That both AGO2^{HALO} constructs generated here interact with TNRC6A suggests that modification of the C-terminus did not impact the fold of the PIWI domain. In line with this, while understanding of the interaction between Dicer and AGO2 is still developing, the PIWI and MID domains are deemed crucial,[66,67,68,69]. This further suggests that the constructs we have produced may have hindered miRNA binding or slicing activity, even though the overall structure of AGO2 and its capacity to recruit functional protein complexes remains largely intact.

Distinct Sub-Cellular Localisation of AGO2^{HALO}

For proteins to function normally, they must localise correctly. We determined from our imaging and fractionation data that sub-cellular localisation of AGO2 is significantly altered as a result of the C-terminal fusion, with a much reduced nuclear localisation of the AGO2 fusion protein in *AGO2*^{HALO} cells (***Fig. 5A-D***). Notably, *Ago2*$^{-/-}$ MEFs expressing an N-terminal HaloTag-Ago2 fusion were also found to show a prevalently cytoplasmic localisation of the fusion protein,[14] though it is unclear if this differs from the signal present in *WT* cells due to a lack of direct comparison. Impaired nuclear localisation could arise for many reasons, most obviously perhaps due to the addition of the large (33 kDa) HaloTag preventing binding of mediators of nuclear import.[70,71] It may also be the case that loss of the carboxylate group of A859 specifically disrupts the structure of AGO2 in a way that impairs binding to nuclear import factors. Factors that regulate nuclear import of AGO2 continue to be revealed[72,73] and it may be that the PIWI domain and/or the C-terminal region are more critical in these interactions than is currently understood. Further studies with deletion mutants of AGO2 would help define the critical residues and structural motifs. Although RISC activity has been considered primarily cytoplasmic, and our principal research intention was to use *AGO2*^{HALO} to investigate (primarily) cytoplasmic RISC activity, nuclear RISC has been shown to regulate both transcriptional rates and post-transcriptional mRNA, and RNAi factors are known to be present and functional in human cell nuclei.[74,75,75,76,77] Moreover, a shift in localization of AGO2 from cytoplasm to nucleus was recently shown to derepress cytoplasmic AGO2-eCLIP targets that were candidates for canonical regulation by miRISC.[63] Therefore, the potential downstream effects of disrupted nuclear localisation should not be overlooked when considering *AGO2*^{HALO} as a model for studying AGO2/RISC.

Previous studies have shown that, in A549 cells, there is a greater, but comparable, concentration of nuclear and cytoplasmic AGO2 and, in most cell types, generally a nuclear to cytoplasmic ratio below one.[77,78] Our fractionation data supports this, with comparable levels of AGO2 observed in both fractions of A549 *WT* cells.

Interestingly, tagged AGO2 has previously been shown to result in altered AGO2 protein localisation. N-terminal tagged FLAG-AGO2 exhibited shifted nuclear and cytoplasmic distribution (approximately equal for endogenous AGO2 in T47D cells compared with 67% cytoplasmic and 33% nuclear in *FLAG-AGO2* over-expressing cells),[8] although this change could be more a consequence of high (5-fold) ectopic overexpression rather than directly attributable to the tag itself. Immunofluorescence images of *MYC-AGO2* U2-OS cells stained with FITC-conjugated anti-Myc showed a predominantly cytoplasmic Myc-AGO2 signal with prevalent cytoplasmic foci, while endogenous AGO2 showed a predominantly nuclear signal – it is uncertain if these differences arise directly from the Myc-tag or non-specific antibody binding.[79] Intriguingly, we observed a contrasting nuclear AGO2 signal when using a Rat anti-AGO2 (displaying weak nuclear signal) versus a Mouse anti-AGO2 (displaying greater nuclear signal) antibody. The HaloTag-TMR signal (which we would expect to be highly specific to the *AGO2*^{HALO} fusion protein) showed a weak nuclear signal, closer to that observed in cells probed with Rat anti-AGO2 antibody. A similar signal was observed for this Rat anti-AGO2 antibody in HeLa cells, with both nuclear and cytoplasmic staining depleting after si*AGO2* knock-down.[80] This observation was particularly curious given the Rat anti-AGO2 antibody associates with chromatin and SWI/SNF in the absence of AGO2 and cross-reacts with SMARCC1, which we would expect to localise to the nucleus.[81] We were unable to find detailed published evidence of non-specific binding for the Mouse anti-AGO2 antibody. If used for immunofluorescence, ChIP-seq, or CLIP-seq (as they have been), either of these two antibodies would likely result in consequential artefact emergence. Re-evaluation of published findings which employed these antibodies may be required, as has already been proposed for the Rat anti-AGO2 11A9 antibody.[81] Indeed, known (and unknown) cross-reactivity of AGO2 antibodies with other components in the cell were a major reason we initially commenced designs to fuse AGO2 with HaloTag. This re-emphasises the need for caution when interpreting previous data and the general need for proper validation when using any type of tag or antibody to investigate the fundamental biology of proteins/complexes such as AGO2 and RISC, as all risk artefact emergence.

Together with our reporter assays indicating significantly impaired silencing function, the distinct sub-cellular localisation of *AGO2-HaloTag* convinced us to reject C-terminal *AGO2*^{HALO} fusion as a viable tool for study of RISC.

Conclusion

The capacity to investigate the mechanisms behind biological processes and disease has been greatly enhanced by the ability to produce proteins of interest fused to relevant tags. However, every tag added to a protein has the potential to impede functionality, which may invalidate any experimental conclusions. As a result, careful tag design together with reliable and reproducible validation experiments are essential for advancing miRNA-silencing research. This is especially important for proteins like AGO2, which often function as part of larger complex and have numerous and diverse roles and activities. Concerningly, several previous studies that have used tagged forms of AGO2 to investigate AGO2/RISC have not adequately demonstrated, either through published tag validation or the lack thereof, that core functions of tagged AGO2 are not impacted. As even small modifications can have functional consequences, this shortfall in validation casts doubt on the validity of some of these findings. Additionally, the paucity of AGO2 antibody validation presents a risk of artificial results arising from non-specific binding of antibodies used to probe AGO2. Therefore, to ensure the validity and robustness of future AGO2/RISC investigational findings, we recommend more comprehensive protein-tag (and antibody) validation work to be performed and published in detail alongside investigational findings.

We constructed C-terminal *AGO2*^{HALO} fusion cells to investigate if AGO2^{HALO} was a suitable model for studying RISC biology in human cells. Our research revealed that, while some normal function is retained with AGO2^{HALO} maintaining capacity to form native protein-protein interactions, *AGO2*^{HALO} cells displayed distinct sub-cellular localization and significantly reduced silencing function compared to normal AGO2. This loss of function led us to conclude that C-terminal fusion of *AGO2*^{HALO} was not appropriate for further research into the biology of AGO2/RISC. Although our study was not comparative and was limited to testing only one type of endogenous

AGO2-tag fusion, the 33 kDa HaloTag, our findings suggest that C-terminal tagging of AGO2 in general may not be advisable.

Ultimately, we hope that our work serves as a valuable case study to underscore the importance of careful validation of all core protein competencies of recombinantly tagged proteins. We strongly encourage future research using N-terminal (or any) AGO2 tag fusions to conduct and publish comprehensive validation assays. It is crucial to avoid relying on any single assay and, instead, perform a combination of experiments (e.g., Luciferase reporter assays, *miR-451a* assays, co-immunoprecipitation experiments, and localization studies) to validate the range of core protein functionalities, thereby increasing confidence in investigational findings. By following these validation strategies, researchers can ensure that their findings related to AGO2 are robust, reliable, and more representative of RNA silencing biology. A community-wide effort to ensure only the most robustly validated reagents and methods are used to characterise AGO2 and RISC biology would enable the miRNA community to gain valuable insights into RNA silencing biology of greater scientific rigour. More broadly, the availability of AlphaFold models for 220 million proteins means that the design of fusion proteins can now be guided by atomic resolution predictions of protein structure in the absence of experimental data. We therefore strongly recommend well-thought-out design and validation strategies to enhance our understanding of the impact of specific tags and tagging strategies on protein function.

Funding

This work was supported by funds awarded to T.V.S. from the BBSRC (Grant Code BB/V009567/1).

Author contributions

K.M.S., A.F.F.C, P.S.R. M.J.P., and T.V.S. designed and performed experiments and analyzed the data. A.A and M.A. provide invaluably technical and experimental assistance. All authors contributed to editing and proofreading the manuscript. K.M.S., A.F.F.C, P.S.R. M.J.P., and T.V.S. wrote the manuscript. T.V.S. supervised and managed all research.

Acknowledgements

We would like to acknowledge the advice and helpful discussions of this work/investigation from Prof. Dimitris Lagos, Dr Faraz Mardakheh and Dr Paul Grevitt.

References

1. Hutvagner, G. & Simard, M. J. Argonaute proteins: Key players in RNA silencing. *Nat. Rev. Mol. Cell Biol.* **9**, 22–32 (2008).

2. Frédérick, P. M. & Simard, M. J. Regulation and different functions of the animal microRNA-induced silencing complex. *Wiley Interdiscip. Rev. RNA* 1–22 (2021) doi:10.1002/wrna.1701.

3. Huntzinger, E. & Izaurralde, E. Gene silencing by microRNAs: Contributions of translational repression and mRNA decay. *Nat. Rev. Genet.* **12**, 99–110 (2011).

4. Behm-Ansmant, I. *et al.* mRNA degradation by miRNAs and GW182 requires both CCR4:NOT deadenylase and DCP1:DCP2 decapping complexes. *Genes Dev.* **20**, 1885–1898 (2006).

5. Chekulaeva, M. *et al.* MiRNA repression involves GW182-mediated recruitment of CCR4-NOT through conserved W-containing motifs. *Nat. Struct. Mol. Biol.* **18**, 1218–1226 (2011).

6. Lian, S. L. *et al.* The C- Terminal half of human Ago2 binds to multiple GW- rich regions of GW182 and requires GW182 to mediate silencing. *Rna* **15**, 804–813 (2009).

7. Liu, J. *et al.* A role for the P-body component GW182 in microRNA function. *Nat. Cell Biol.* **7**, 1161–1166 (2005).

8. Roya, K. *et al.* Stable association of RNAi machinery is conserved between the cytoplasm and nucleus of human cells. *Rna* **22**, 1085–1098 (2016).

9. Mauro, M., Berretta, M., Palermo, G., Cavalieri, V. & Rocca, G. La. Special Section on Non-Coding RNAs in Clinical Practice : From Biomarkers to Therapeutic Tools — Minireview The Multiplicity of Argonaute Complexes in Mammalian Cells. *J. Pharmacol. Exp. Ther.* 52–60 (2023) doi:10.1124.

10. Kedersha, N. & Anderson, P. Mammalian Stress Granules and Processing Bodies. *Methods Enzymol.* **431**, 61–81 (2007).

11. Gibson, T. J., Seiler, M. & Veitia, R. A. The transience of transient overexpression. *Nat. Methods* **10**, 715–721 (2013).

12. Booth, W. T. *et al.* Impact of an N terminal polyhistidine tag on protein thermal stability. *ACS Omega* **3**, 760–768 (2018).

13. La Rocca, G. *et al.* In vivo, Argonaute-bound microRNAs exist predominantly in a reservoir of low molecular weight complexes not associated with mRNA. *Proc. Natl. Acad. Sci. U. S. A.* **112**, 767–772 (2015).

14. Li, X. *et al.* High-Resolution In Vivo Identification of miRNA Targets by Halo-Enhanced Ago2 Pull-Down. *Mol. Cell* **79**, 167-179.e11 (2020).

15. Horman, S. R. *et al.* Akt-mediated phosphorylation of argonaute 2 downregulates cleavage and upregulates translational repression of MicroRNA targets. *Mol. Cell* **50**, 356–367 (2013).

16. Gurard-levin, Z. A., Kilian, K. A., Kim, J. & Ba, K. HaloTag: A Novel Protein Labeling Technology for Cell Imaging and Protein Analysis. *ACS Chem. Biol.* **60**, 45–58 (2010).

17. England, C. G., Luo, H. & Cai, W. HaloTag Technology: A Versatile Platform for Biomedical Applications. *Bioconjug. Chem.* **26**, 975–986 (2015).

18. Chen, W., YOUNIS, M. H., Zhao, Z. & Cai, W. Recent biomedical advances enabled by HaloTag technology. *Biocell* **46**, 1789–1801 (2022).

19. Gu, J. *et al.* GoldCLIP: Gel-omitted Ligation-dependent CLIP. *Genomics, Proteomics Bioinforma.* **16**, 136–143 (2018).

20. Hafner, M. *et al.* CLIP and complementary methods. *Nat. Rev. Methods Prim.* **1**, (2021).

21. Grimm, J. B. *et al.* A general method to improve fluorophores for live-cell and single-molecule microscopy. *Nat. Methods* **12**, 244–250 (2015).

22. Duc, H. & Ren, X. Labelling HaloTag Fusion Proteins with HaloTag Ligand in Living Cells. *Bio-Protocol* **7**, 1–8 (2017).

23. Kompa, J. *et al.* Exchangeable HaloTag Ligands (xHTLs) for multi-modal super-resolution fluorescence microscopy. *J. Am. Chem. Soc.* 2022.06.20.496706 (2022) doi:10.1021/jacs.2c11969.

24. Kwak, P. B. & Tomari, Y. The N domain of Argonaute drives duplex unwinding during RISC assembly. *Nat. Struct. Mol. Biol.* **19**, 145–151 (2012).

25. Ma, J. B., Ye, K. & Patel, D. J. Structural basis for overhang-specific small interfering RNA recognition by the PAZ domain. *Nature* **429**, 318–322 (2004).

26. Gu, S., Jin, L., Huang, Y., Zhang, F. & Kay, M. A. Slicing-independent RISC activation requires the argonaute PAZ domain. *Curr. Biol.* **22**, 1536–1542 (2012).

27. Boland, A., Huntzinger, E., Schmidt, S., Izaurralde, E. & Weichenrieder, O. Crystal structure of the MID-PIWI lobe of a eukaryotic argonaute protein. *Proc. Natl. Acad. Sci. U. S. A.* **108**, 10466–10471 (2011).

28. Parker, J. S., Roe, S. M. & Barford, D. Structural insights into mRNA recognition from a PIWI domain-siRNA guide complex. *Nature* **434**, 663–666 (2005).

29. Song, J. J., Smith, S. K., Hannon, G. J. & Joshua-Tor, L. Crystal structure of argonaute and its implications for RISC slicer activity. *Science (80-.).* **305**, 1434–1437 (2004).

30. Parker, J. S., Roe, S. M. & Barford, D. Crystal structure of a PIWI protein suggests mechanisms for siRNA recognition and slicer activity. *EMBO J.* **23**, 4727–4737 (2004).

31. Ma, J. B. *et al.* Structural basis for 5′-end-specific recognition of guide RNA by the A. fulgidus Piwi protein. *Nature* **434**, 666–670 (2005).

32. Rivas, F. V. *et al.* Purified Argonaute2 and an siRNA form recombinant human RISC. *Nat. Struct. Mol. Biol.* **12**, 340–349 (2005).

33. Kang, H. W., Tabata, Y. & Ikada, Y. Fabrication of porous gelatin scaffolds for tissue engineering. *Biomaterials* (1999) doi:10.1016/S0142-9612(99)00036-8.

34. Yuan, Y. R. *et al.* Crystal structure of A. aeolicus argonaute, a site-specific DNA-guided endoribonuclease, provides insights into RISC-mediated mRNA cleavage. *Mol. Cell* **19**, 405–419 (2005).

35. Nakanishi, K., Weinberg, D. E., Bartel, D. P. & Patel, D. J. Structure of yeast Argonaute with guide RNA. *Nature* **486**, 368–374 (2012).

36. Nakanishi, K. Critical Reviews and Perspectives Anatomy of four human Argonaute proteins. 1–21 (2022).

37. Müller, M., Fazi, F. & Ciaudo, C. Argonaute Proteins: From Structure to Function in Development and Pathological Cell Fate Determination. *Front. Cell Dev. Biol.* **7**, 1–10 (2020).

38. Hauptmann, J. *et al.* Turning catalytically inactive human Argonaute proteins into active slicer enzymes. *Nat. Struct. Mol. Biol.* **20**, 814–817 (2013).

39. Schürmann, N., Trabuco, L. G., Bender, C., Russell, R. B. & Grimm, D. Molecular dissection of human Argonaute proteins by DNA shuffling. *Nat. Struct. Mol. Biol.* **20**, 818–826 (2013).

40. Hur, J. K., Zinchenko, M. K., Djuranovic, S. & Green, R. Regulation of Argonaute slicer activity by guide RNA 3′ end interactions with the N-terminal lobe. *J. Biol. Chem.* **288**, 7829–7840 (2013).

41. Mukherji, S. *et al.* MicroRNAs can generate thresholds in target gene expression. *Nat. Genet.* **43**, 854–859 (2011).

42. Schmid-Burgk, J. L., Höning, K., Ebert, T. S. & Hornung, V. CRISPaint allows modular base-specific gene tagging using a ligase-4-dependent mechanism. *Nat. Commun.* **7**, (2016).

43. Liu, Z., Johnson, S. T., Zhang, Z. & Corey, D. R. Expression of TNRC6 (GW182) Proteins Is Not Necessary for Gene Silencing by Fully Complementary RNA Duplexes. *Nucleic Acid Ther.* **29**, 323–334 (2019).

44. Jumper, J. *et al.* Highly accurate protein structure prediction with AlphaFold. *Nature* **596**, 583–589 (2021).

45. Mirdita, M. *et al.* ColabFold: making protein folding accessible to all. *Nat. Methods* **19**, 679–682 (2022).

46. Cavallo, L., Kleinjung, J. & Fraternali, F. POPS: A fast algorithm for solvent accessible surface areas at atomic and residue level. *Nucleic Acids Res.* **31**, 3364–3366 (2003).

47. Elkayam, E. *et al.* The structure of human argonaute-2 in complex with miR-20a. *Cell* **150**, 100–110 (2012).

48. Hug, N., Longman, D. & Cáceres, J. F. Mechanism and regulation of the nonsense-mediated decay pathway. *Nucleic Acids Res.* **44**, 1483–1495 (2015).

49. Johnson, K. C., Johnson, S. T., Liu, J. & Chu, Y. Prioritizing Annotated miRNAs: Only a Small Percentage are Candidates for Biological Regulation. (2022).

50. Chendrimada, T. P. *et al.* TRBP recruits the Dicer complex to Ago2 for microRNA processing and gene silencing. *Nature* **436**, 740–744 (2005).

51. Cheloufi, S., Dos Santos, C. O., Chong, M. M. W. & Hannon, G. J. A dicer-independent miRNA biogenesis pathway that requires Ago catalysis. *Nature* **465**, 584–589 (2010).

52. Cifuentes, D. *et al.* A novel miRNA processing pathway independent of dicer requires argonaute2 catalytic activity. *Science (80-.).* **328**, 1694–1698 (2010).

53. Yang, S. *et al.* Conserved vertebrate mir-451 provides a platform for Dicer-independent, Ago2-mediated microRNA biogenesis. *Proc. Natl. Acad. Sci. U. S. A.* **107**, 15163–15168 (2010).

54. Kretov, D. A. *et al.* Ago2-Dependent Processing Allows miR-451 to Evade the Global MicroRNA Turnover Elicited during Erythropoiesis. *Mol. Cell* **78**, 317-328.e6 (2020).

55. Hwang, H., Wentzel, E. A. & Mendell, J. T. Cell-cell contact globally activates microRNA biogenesis. (2009).

56. Sato, H. & Singer, R. H. Cellular variability of nonsense-mediated mRNA decay. *Nat. Commun.* **12**, 1–12 (2021).

57. Choe, J., Cho, H., Lee, H. C. & Kim, Y. K. MicroRNA/Argonaute 2 regulates nonsense-mediated messenger RNA decay. *EMBO Rep.* **11**, 380–386 (2010).

58. Choe, J., Cho, H., Chi, S. G. & Kim, Y. K. Ago2/miRISC-mediated inhibition of CBP80/20-dependent translation and thereby abrogation of nonsense-mediated mRNA decay require the cap-associating activity of Ago2. *FEBS Lett.* **585**, 2682–2687 (2011).

59. Park, S. Y., Choi, H. C., Chun, Y. H., Kim, H. & Park, S. H. Characterization of chromosomal aberrations in lung cancer cell lines by cross-species color banding. *Cancer Genet. Cytogenet.* **124**, 62–70 (2001).

60. Bian, X. J. *et al.* Down-regulation of Dicer and Ago2 is associated with cell proliferation and apoptosis in prostate cancer. *Tumor Biol.* **35**, 11571–11578 (2014).

61. Schirle, N. T. & MacRae, I. J. The crystal structure of human argonaute2. *Science (80-.).* **336**, 1037–1040 (2012).

62. Sheu-Gruttadauria, J. & MacRae, I. J. Phase Transitions in the Assembly and Function of Human miRISC. *Cell* **173**, 946-957.e16 (2018).

63. Johnson, K. C., Kilikevicius, A., Hofman, C., Hu, J. & Liu, Y. Nuclear Localization of Argonaute is affected by Cell Density and May Relieve Repression by microRNAs. (2023).

64. Jacob, E. & Unger, R. A tale of two tails: Why are terminal residues of proteins exposed? *Bioinformatics* **23**, 225–230 (2007).

65. Akdel, M. *et al.* A structural biology community assessment of AlphaFold2 applications. *Nat. Struct. Mol. Biol.* **29**, 1056–1067 (2022).

66. Sasaki, T. & Shimizu, N. Evolutionary conservation of a unique amino acid sequence in human DICER protein essential for binding to Argonaute family proteins. *Gene* **396**, 312–320 (2007).

67. Doi, N. *et al.* Short-interfering-RNA-mediated gene silencing in mammalian cells requires dicer and eIF2C translation initiation factors. *Curr. Biol.* **13**, 41–46 (2003).

68. Tahabaz, N. *et al.* Characterization of the interactions between mammalian PAZ PIWI domain proteins and Dicer. *EMBO Rep.* **5**, 189–194 (2004).

69. Wang, H. W. *et al.* Structural insights into RNA processing by the human RISC-loading complex. *Nat. Struct. Mol. Biol.* **16**, 1148–1153 (2009).

70. Sallis, S., Grondin, B., Leduc, E., Azouz, F. & Pilon, N. FAM172A controls the nuclear import and alternative splicing function of AGO2. *bioRxiv* (2022).

71. Schraivogel, D. *et al.* Importin-β facilitates nuclear import of human GW proteins and balances cytoplasmic gene silencing protein levels. *Nucleic Acids Res.* **43**, 7447–7461 (2015).

72. Weinmann, L. *et al.* Importin 8 Is a Gene Silencing Factor that Targets Argonaute Proteins to Distinct mRNAs. *Cell* **136**, 496–507 (2009).

73. Sallis, S. *et al.* The CHARGE syndrome-associated protein FAM172A controls AGO2 nuclear import. *Life Sci. alliance* **6**, 1–15 (2023).

74. O'Brien, J., Hayder, H., Zayed, Y. & Peng, C. Overview of microRNA biogenesis, mechanisms of actions, and circulation. *Front. Endocrinol. (Lausanne).* **9**, 1–12 (2018).

75. Nishi, K., Nishi, A., Nagasawa, T. & Ui-Tei, K. Human TNRC6A is an Argonaute-navigator protein for microRNA-mediated gene silencing in the nucleus. *Rna* **19**, 17–35 (2013).

76. Pitchiaya, S., Heinicke, L. A., Park, J. I., Cameron, E. L. & Walter, N. G. Resolving Subcellular miRNA Trafficking and Turnover at Single-Molecule Resolution. *Cell Rep.* **19**, 630–642 (2017).

77. Gagnon, K. T., Li, L., Chu, Y., Janowski, B. A. & Corey, D. R. RNAi factors are present and active in human cell nuclei. *Cell Rep.* **6**, 211–221 (2014).

78. Sarshad, A. A. *et al.* Argonaute-miRNA Complexes Silence Target mRNAs in the Nucleus of Mammalian Stem Cells. *Mol. Cell* **71**, 1040-1050.e8 (2018).

79. Liu, J., Valencia-Sanchez, M. A., Hannon, G. J. & Parker, R. MicroRNA-dependent localization of targeted mRNAs to mammalian P-bodies. *Nat. Cell Biol.* **7**, 719–723 (2005).

80. Rüdel, S., Flatley, A., Weinmann, L., Kremmer, E. & Meister, G. A multifunctional human Argonaute2-specific monoclonal antibody. *Rna* **14**, 1244–1253 (2008).

81. Van Eijl, R. A. P. M., Van Den Brand, T., Nguyen, L. N. & Mulder, K. W. Reactivity of human AGO2 monoclonal antibody 11A9 with the SWI/SNF complex: A case study for rigorously defining antibody selectivity. *Sci. Rep.* **7**, 1–11 (2017).

Figure Legends

Figure 1. Creation and Genomic Characterisation of AGO2-HaloTag Cell Lines

(A) Schematic of the three-plasmid tagging system used to generate C terminal *AGO2-HaloTag* fusion cells. (B) Schematic of WT AGO2 and the C terminal AGO2-HaloTag fusion (including T2A site, Puromycin resistant (PuroR) and Poly(A) sections) genotype to be generated by CRISPaint editing of A549 cells. Arrows indicate locations of forward and reverse primers designed to confirm editing. Blue = *AGO2* WT last intron Forward and Reverse; Light Teal = HaloTag1 Forward and Reverse; Dark Teal = HaloTag2 Forward and Reverse. (C) Experimental design employed to generate and select *AGO2-HaloTag* (and non-transfected (*UnTagged*)) CRISPaint clones. D) Agarose gel loaded with PCR products of A549 WT and two *AGO2-HaloTag* (*AGO2-HaloTag C5* and *AGO2-HaloTag C10*) lines amplified with indicated combinations of *AGO2* WT and *HaloTag* primers, as indicated in (B). Red arrows indicate gDNA containing *HaloTag* sequence which was purified and submitted for sequencing. Circled numbers 1-3 indicate gDNA containing C terminal non-HaloTagged *AGO2* product which was purified and submitted for sequencing. (E) Sequence (generated from TOPO-seq) alignments of *WT* and two *AGO2-HaloTag* clones at the AGO2-HaloTag junction. From several submitted TOPO clones, two variants of *AGO2-HaloTag* (one long and one short) were identified in *AGO2-HaloTag* cells. Asterisk (*) indicates STOP codon. (F) Schematic to show known functionally important domains of AGO2, with a focus on C-terminal PIWI domain. CRISPaint mediated AGO2-HaloTag fusion generated a long and a short variant, neither of which resulted in loss of residues known to have functional importance. (G) Chromatograph of C terminal *AGO2* sequence identified in WT, *AGO2-HaloTag C5* and *AGO2-HaloTag C10* cells (Circled numbers 1-3 in (**D**)) showing the additional and premature STOP codon in both *AGO2-HaloTag* lines. (H) Abundance of non-HaloTagged *AGO2* mRNA transcript in A549 WT, two *UnTagged* (*UT C1* and *UT C2*) and two *AGO2-HaloTag* (*AGO2-HaloTag C5* and *AGO2-HaloTag C10*) cells. *AGO2* (non-HaloTagged) mRNA abundance normalised to *B Actin* mRNA abundance and made relative to levels in WT cells. Data represent mean ± SEM; n = 3 (*p ≤ 0.05; **p ≤ 0.01; ***p ≤ 0.001). (I) Western blot of whole-cell lysates from A549 WT, two *UnTagged* (*UT C1* and *UT C2*) and two *AGO2-HaloTag* (*AGO2-HaloTag C5* and *AGO2-HaloTag C10*) cell lines probed with antibodies against AGO2, HaloTag, and Vinculin.

Figure 2. Initial Characterisation of AGO2-HaloTag Cells Lines Indicates AGO2-HaloTag Fusion Results in Tolerable Changes to miRISC Abundance

(A) Doubling time of A549 WT, two *UnTagged* (*UT C1* and *UT C2*) and two *AGO2-HaloTag* (*AGO2-HaloTag C5* and *AGO2-HaloTag C10*) measured using IncucyteZoom over 108 hours. Data represent mean ± SEM; n = 3 (ns p > 0.05).
(B) Representative Western blot of whole-cell lysates from indicated cell lines (harvested during log-phase) probed with antibodies against AGO1, AGO2 (same image as in *Fig. 1I*), AGO4, Vinculin, and Beta Actin.
(C) Densitometry of AGO1/2/4 (normalised to loading control (Vinculin)) in indicated cell lines. Data represent mean ± SEM; n = 3 (*p ≤ 0.05; **p ≤ 0.01; ***p ≤ 0.001).
(D) Representative Western blot of whole-cell lysates from indicated cell lines (harvested during log-phase) probed with antibodies against DDX6, TNRC6A, LIMD1, and Beta Actin.
(E) Densitometry analysis of DDX6, TNRC6A, and LIMD1 (normalised to loading control (Beta Actin)) in indicated cell lines. Data represent mean ± SEM; n = 3 (*p ≤ 0.05; **p ≤ 0.01; ***p ≤ 0.001).

Figure 3. AGO2-HaloTag Has Comparable Binding to TNRC6A and Increased Binding to Dicer compared with untagged AGO2.

(A) Endogenous co-immunoprecipitation of AGO2 with Dicer and TNRC6A in *UnTagged C2 and AGO2-HaloTag C10* cells. Note the observed co-immunoprecipitation of Dicer with AGO2 in *AGO2-HaloTag C10,* but not *UnTagged C2*, cells.
(B) Endogenous co-immunoprecipitation of AGO2 with Dicer in WT and two *AGO2-HaloTag* lines. Note again the observed co-immunoprecipitation of Dicer to AGO2 in *AGO2-HaloTag C5 and C10*, but not WT, cells

Figure 4. AGO2-HaloTag Fusion Impairs AGO2 Cleavage and Silencing Function
(A) *MiR-451a* abundance (normalized to *U6* RNA and made relative to relevant WT) in indicated cell lines lysed during the log phase of growth or at confluency, as indicated, measured by RT-qPCR using the $2^{-\Delta\Delta Ct}$ method. Data represent mean ± SEM; n = 2 (*p ≤ 0.05; **p ≤ 0.01; ***p ≤ 0.001).
(B) Relative derepression of psiCHECK-2-let-7a-mi6 luciferase reporter in indicated cells treated with 30 nM non targeting control (scRNA) or si*AGO2*. De-repression (si*AGO2* / scRNA) calculated from normalized Renilla/Firefly luciferase (RLuc/FFLuc) activity of transfected target and non-targeting reporter plasmids (psiCHECK-2-let-7a-mi6 activity / psiCHECK-2-V_0 activity). Data represent mean ± SEM; n = 3 (ns p > 0.05; *p ≤ 0.05; **p ≤ 0.01).
(C) Relative Firefly / Renilla Luciferase Activity in indicated cell lines transfected with reporter plasmids expressing Firefly and Renilla luciferase and a siRNA against Firefly Luciferase (esi*FFLuc*) or "non-targeting" control (esi*GFP*). The ratio between Firefly and Renilla luciferase activity was measured 24 h after transfection. Data represent mean ± SEM; n = 3 (ns p > 0.05; **p ≤ 0.01;).

Figure 5. AGO2-HaloTag Fusion Protein Has a Distinct Sub-Cellular Localisation
(A) *UnTagged* C1 and *AGO2-HaloTag C10* cells treated with 100 nM HaloTag-TMR ligand (and fixed and stained with mouse anti-AGO2 antibody) visualized using confocal microscopy. Note the prevalently cytoplasmic localization of the HaloTag-TMR ligand signal in *AGO2-HaloTag C10* cell which is distinct from the mouse anti-AGO2 IF signal.
(B) *UnTagged* C1 and *AGO2-HaloTag C10* fixed and stained with rat anti-AGO2 antibody and visualized using confocal microscopy. Note the prevalently cytoplasmic localization of the antibody in *UnTagged* C1 and *AGO2-HaloTag C10* cells, distinct from the mouse anti-AGO2 IF signal in Figure 5A.
(C) Ratio of nuclear:cytoplasmic signal intensities (per cell) of *UnTagged C1* and *AGO2-HaloTag C10* cells probed with one of Mouse anti-AGO2, Rat anti-AGO2, or TMRDirect-HaloTag. Data represent mean (of 3 individual cells signal intensity ratios per condition) ± SD; n = 3 (*p ≤ 0.05).
(D) Lysates of nuclear and cytoplasmic fractions from indicated cell lines probed with antibodies against AGO2, HaloTag, Alpha Tubulin (cytoplasmic marker), and Histone H3 (nuclear marker). Note the presence of AGO2 in WT and *UnTagged* cells, lacking in *AGO2-HaloTag* cells. Also note the residual AGO2 signal at 97 kDa (indicated by arrow) in the cytoplasmic fractions of *AGO2-HaloTag* cells

Figure 6. Structural Insights of the C-terminal of AGO2 for an Explanation of Impaired Function Upon Halotag Insertion
(A) Schematic composition of AGO2 showing 7 main domains and motifs.

(B) C-terminal residue A859 contributes to miRNA binding (PDB code: 4OLB). Residues shown in stick format and residue type and sequence number annotated. Dashed lines show inter-atom distances < 5.0 Å.

(C) Surface representation of AGO2 (4OLB) with domains coloured as in (A). Bound miRNA shown in spheres with 5′-3′ direction indicated. The approximate location of the buried C-terminal residue A859 is indicated.

(D) Surface representation of AGO2 (4OLB) showing sites of tryptophan binding and the N-terminal most residue (A22) seen in the electron density. Residues 1-21 were not observed in the data.

Supplementary Figure 1. STR Profiling for Cell Line Authentication.
A) Genetic characteristics of indicated cell lines were investigated by STR profiling using 16 independent PCR-systems.
Cell Line Authentication Test, Eurofins Genomics Europe Applied Genomics GmbH, Anzinger Str. 7 a, D-85560 Ebersberg
Method: DNA isolation carried out from cell pellet (cell layer). Genetic characteristics were determined by PCR-single-locus-technology. 16 independent PCR-systems D8S1179, D21S11, D7S820, CSF1PO, D3S1358, TH01, D13S317, D16S539, D2S1338, AMEL, D5S818, FGA, D19S433, vWA, TPOX and D18S51 were investigated. In parallel, positive and negative controls were carried out, yielding correct results.
-* no result / weak signal.

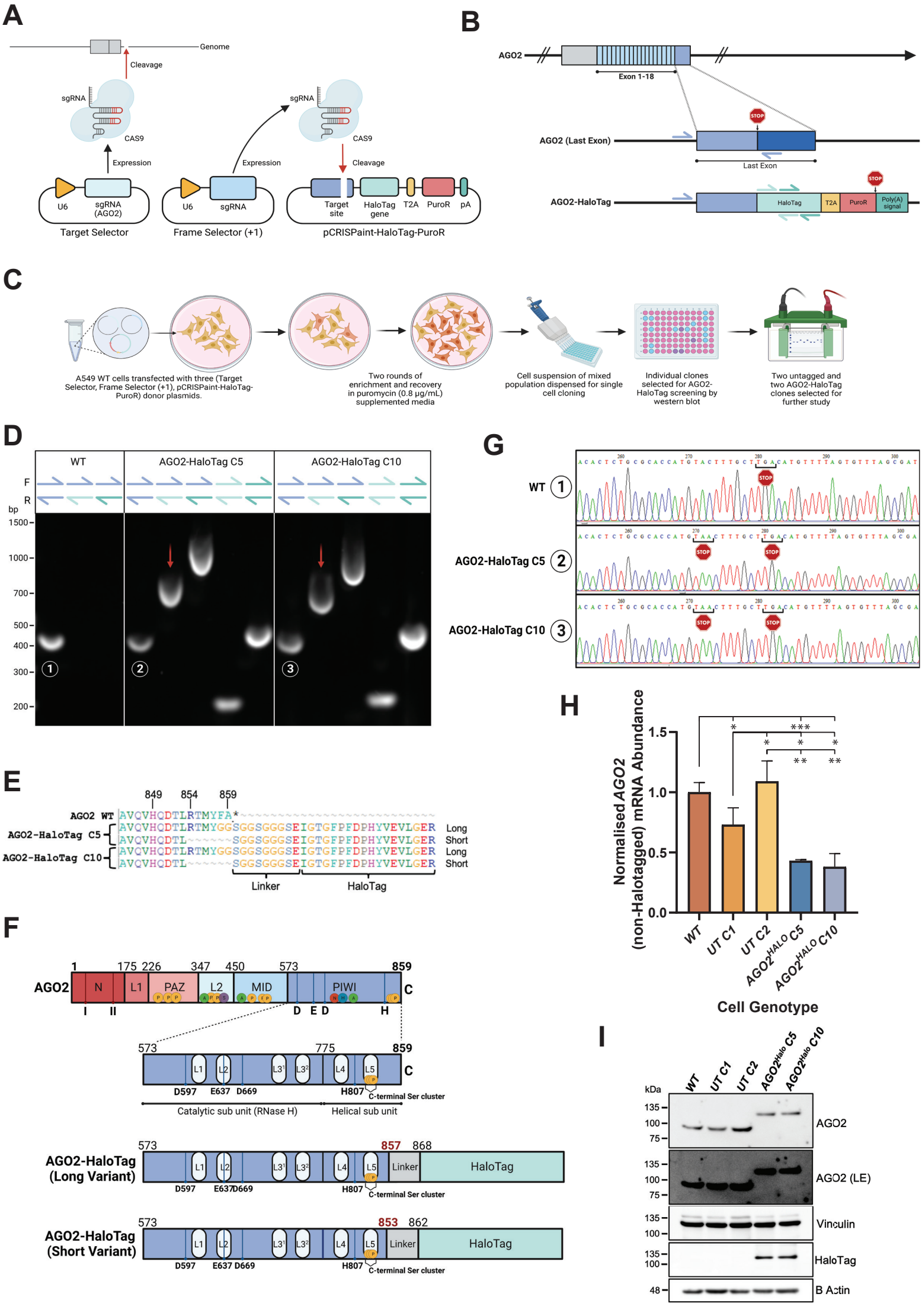
A
Genome
Cleavage
sgRNA
CAS9
Expression
U6
sgRNA (AGO2)
Target Selector
sgRNA
Expression
U6
sgRNA
Frame Selector (+1)
sgRNA
CAS9
Cleavage
Target site
HaloTag gene
T2A
PuroR
pA
pCRISPaint-HaloTag-PuroR
B
AGO2
Exon 1-18
STOP
AGO2 (Last Exon)
Last Exon
AGO2-HaloTag
HaloTag
T2A
PuroR
Poly(A) signal
C
A549 WT cells transfected with three (Target Selector, Frame Selector (+1), pCRISPaint-HaloTag-PuroR) donor plasmids.
Two rounds of enrichment and recovery in puromycin (0.8 µg/mL) supplemented media
Cell suspension of mixed population dispensed for single cell cloning
Individual clones selected for AGO2-HaloTag screening by western blot
Two untagged and two AGO2-HaloTag clones selected for further study
D
WT
AGO2-HaloTag C5
AGO2-HaloTag C10
F
R
bp
1500
1000
700
500
400
300
200
1
2
3
G
WT 1
AGO2-HaloTag C5 2
AGO2-HaloTag C10 3
STOP
E
849 854 859
AGO2 WT AVQVHQDTLRTMYFA*
AGO2-HaloTag C5 AVQVHQDTLRTMYGGSGGSGGGSEIGTGFPFDPHYVEVLGER Long
AVQVHQDTL~~~~~SGGSGGGSEIGTGFPFDPHYVEVLGER Short
AGO2-HaloTag C10 AVQVHQDTLRTMYGGSGGSGGGSEIGTGFPFDPHYVEVLGER Long
AVQVHQDTL~~~~~SGGSGGGSEIGTGFPFDPHYVEVLGER Short
Linker
HaloTag
H
Normalised AGO2 (non-Halotagged) mRNA Abundance
1.5
1.0
0.5
0.0
WT
UT C1
UT C2
AGO2HALO C5
AGO2HALO C10
Cell Genotype
F
AGO2
1 175 226 347 450 573 859
N L1 PAZ L2 MID PIWI C
I II D E D H
573 775 859
L1 L2 L3¹ L3² L4 L5 C
D597 E637 D669 H807 C-terminal Ser cluster
Catalytic sub unit (RNase H)
Helical sub unit
AGO2-HaloTag (Long Variant)
573 857 868
L1 L2 L3¹ L3² L4 L5 Linker HaloTag
D597 E637 D669 H807 C-terminal Ser cluster
AGO2-HaloTag (Short Variant)
573 853 862
L1 L2 L3¹ L3² L4 L5 Linker HaloTag
D597 E637 D669 H807 C-terminal Ser cluster
I
kDa
WT
UT C1
UT C2
AGO2Halo C5
AGO2Halo C10
135
100
75
AGO2
AGO2 (LE)
Vinculin
HaloTag
48
B Actin

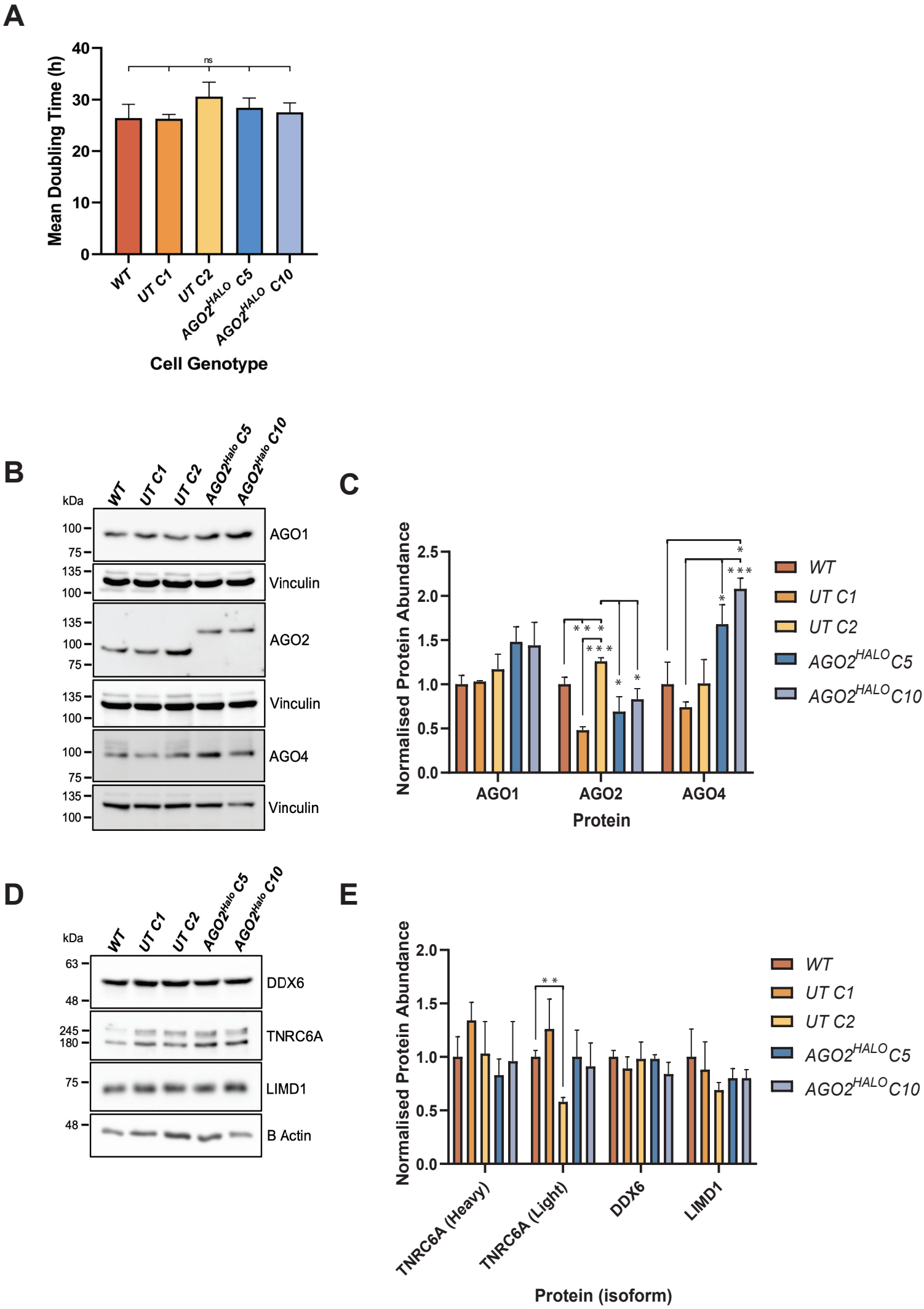
A
Mean Doubling Time (h)
40
30
20
10
0
ns
WT
UT C1
UT C2
AGO2HALO C5
AGO2HALO C10
Cell Genotype
B
kDa
WT
UT C1
UT C2
AGO2Halo C5
AGO2Halo C10
100
75
AGO1
135
100
Vinculin
135
100
75
AGO2
135
100
Vinculin
100
75
AGO4
135
100
Vinculin
C
Normalised Protein Abundance
2.5
2.0
1.5
1.0
0.5
0.0
AGO1
AGO2
AGO4
Protein
WT
UT C1
UT C2
AGO2HALO C5
AGO2HALO C10
D
kDa
WT
UT C1
UT C2
AGO2Halo C5
AGO2Halo C10
63
48
DDX6
245
180
TNRC6A
75
LIMD1
48
B Actin
E
Normalised Protein Abundance
2.0
1.5
1.0
0.5
0.0
TNRC6A (Heavy)
TNRC6A (Light)
DDX6
LIMD1
Protein (isoform)
WT
UT C1
UT C2
AGO2HALO C5
AGO2HALO C10

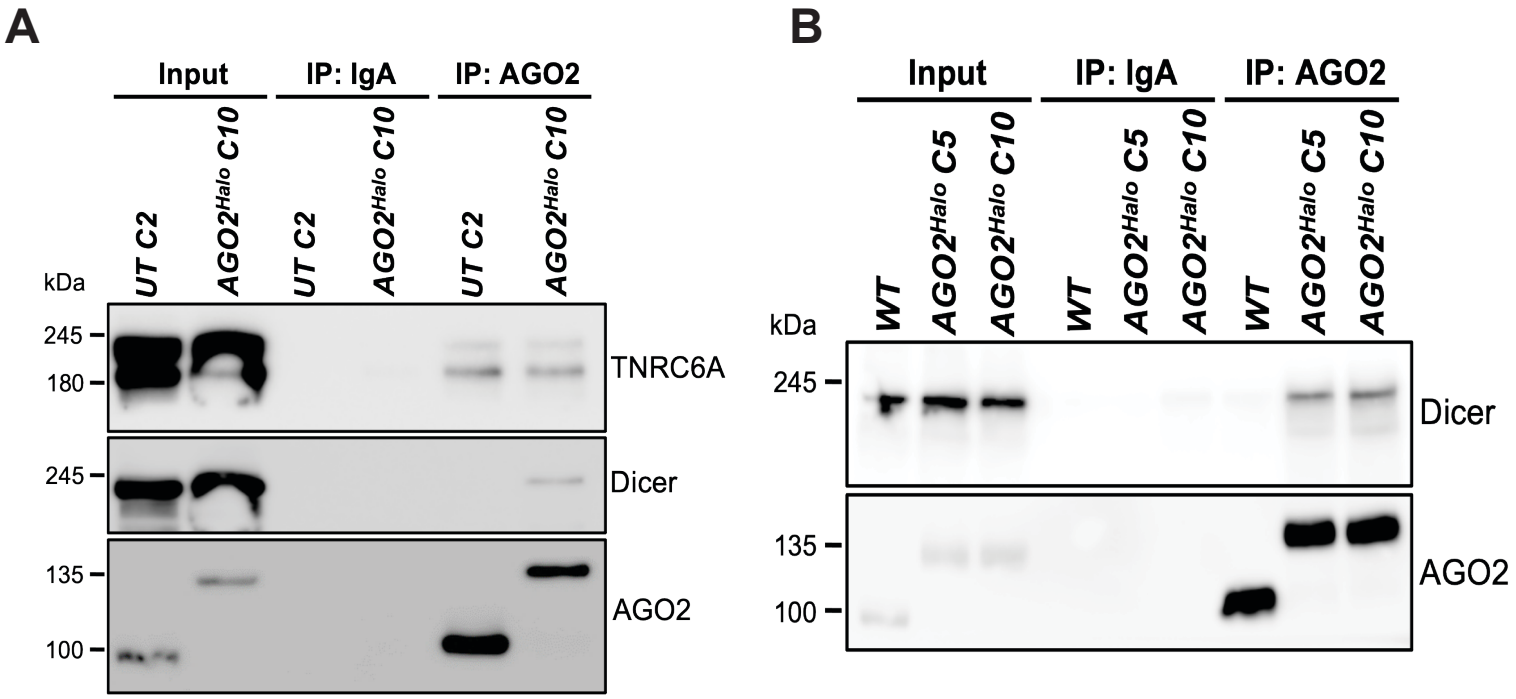
A
Input
IP: IgA
IP: AGO2
UT C2
AGO2Halo C10
UT C2
AGO2Halo C10
UT C2
AGO2Halo C10
kDa
245
180
TNRC6A
245
Dicer
135
100
AGO2
B
Input
IP: IgA
IP: AGO2
WT
AGO2Halo C5
AGO2Halo C10
WT
AGO2Halo C5
AGO2Halo C10
WT
AGO2Halo C5
AGO2Halo C10
kDa
245
Dicer
135
100
AGO2

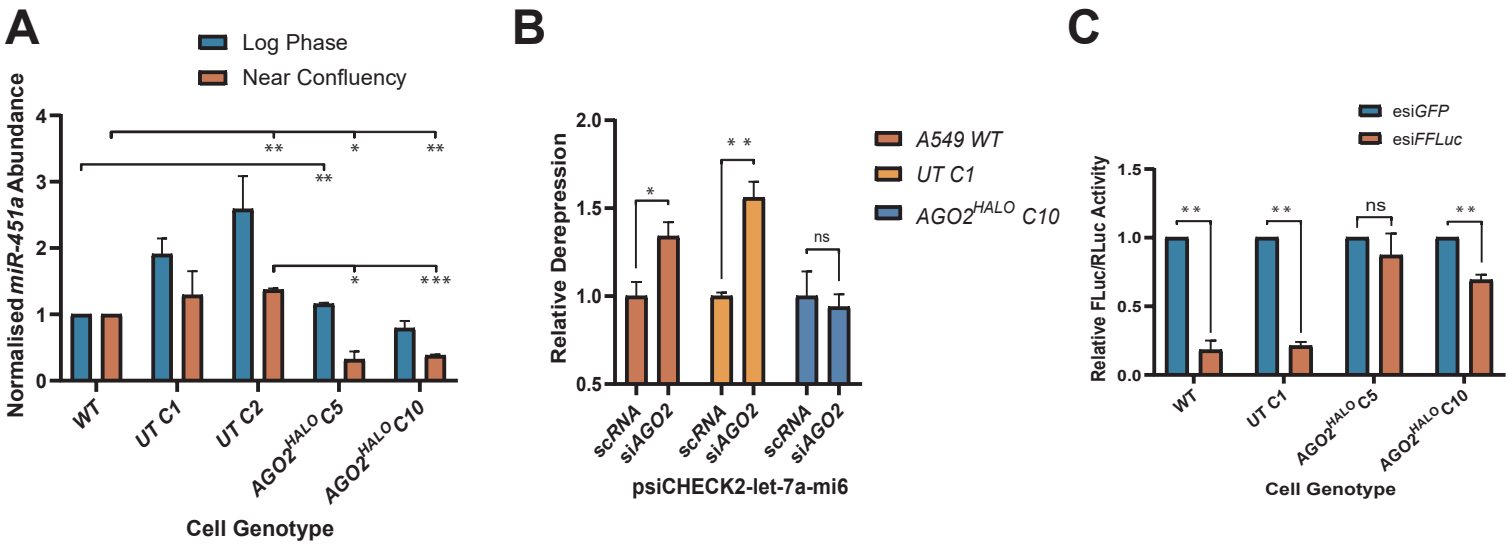
A
Log Phase
Near Confluency
Normalised miR-451a Abundance
0
1
2
3
4
**
*
**
**
*
***
WT
UT C1
UT C2
AGO2HALO C5
AGO2HALO C10
Cell Genotype
B
A549 WT
UT C1
AGO2HALO C10
Relative Derepression
0.5
1.0
1.5
2.0
*
* *
ns
scRNA
siAGO2
psiCHECK2-let-7a-mi6
C
esiGFP
esiFFLuc
Relative FLuc/RLuc Activity
0.0
0.5
1.0
1.5
* *
* *
ns
* *
WT
UT C1
AGO2HALO C5
AGO2HALO C10
Cell Genotype

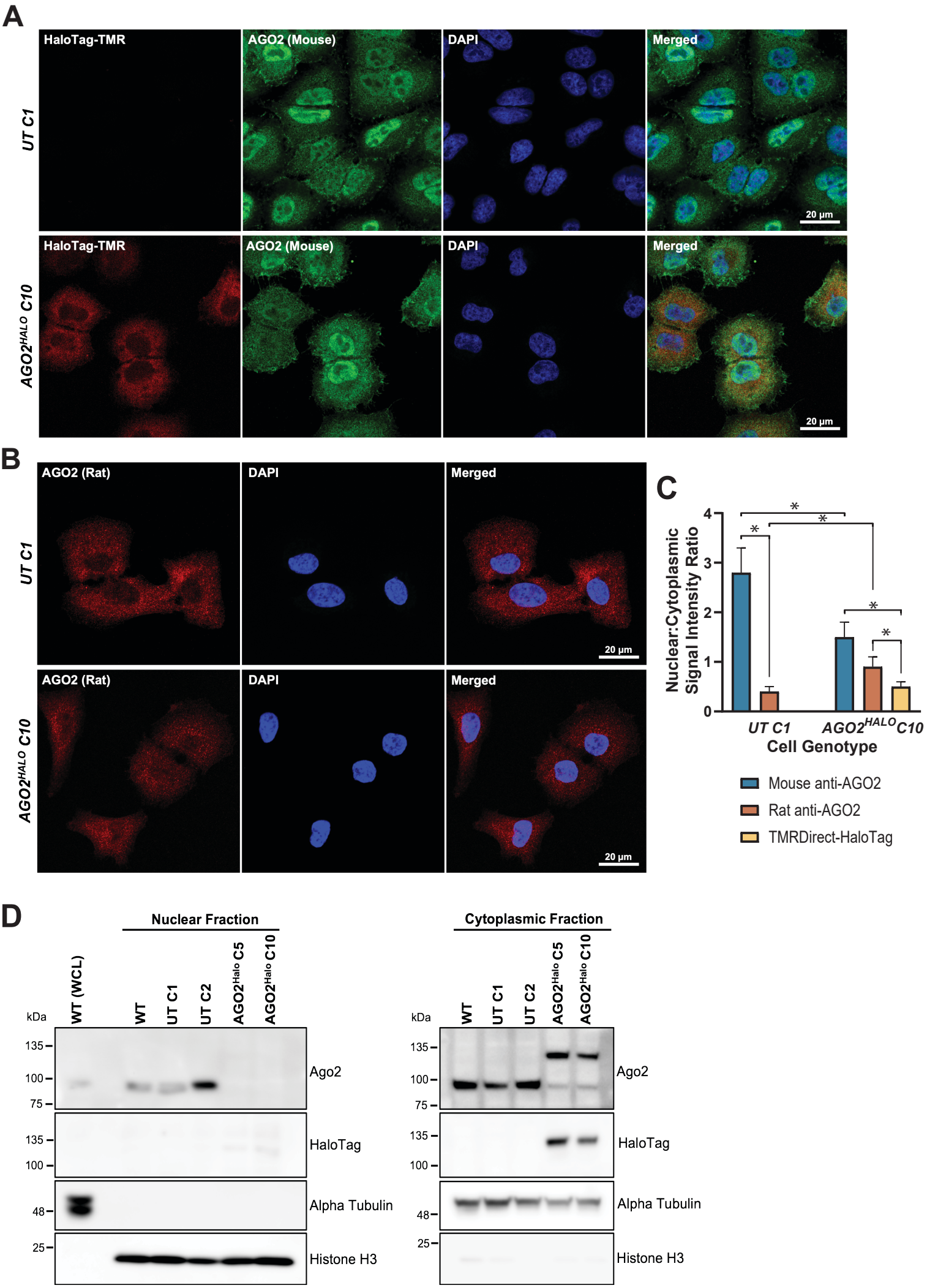
A
HaloTag-TMR
AGO2 (Mouse)
DAPI
Merged
UT C1
AGO2HALO C10
20 µm
B
AGO2 (Rat)
C
Nuclear:Cytoplasmic Signal Intensity Ratio
Cell Genotype
Mouse anti-AGO2
Rat anti-AGO2
TMRDirect-HaloTag
D
Nuclear Fraction
Cytoplasmic Fraction
WT (WCL)
WT
UT C1
UT C2
AGO2Halo C5
AGO2Halo C10
kDa
Ago2
HaloTag
Alpha Tubulin
Histone H3

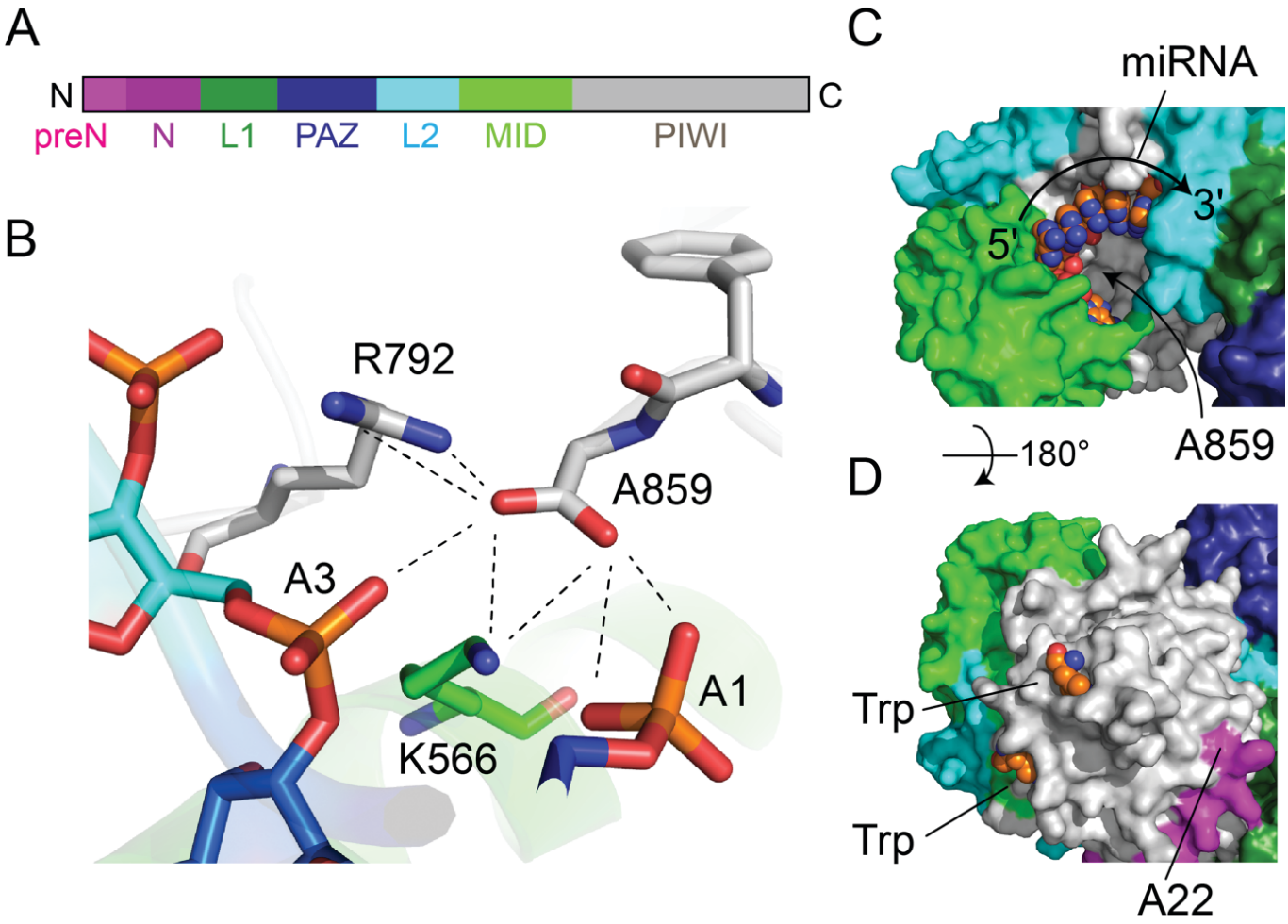
A
N
C
preN
N
L1
PAZ
L2
MID
PIWI
B
R792
A859
A3
A1
K566
C
miRNA
5'
3'
A859
180°
D
Trp
Trp
A22